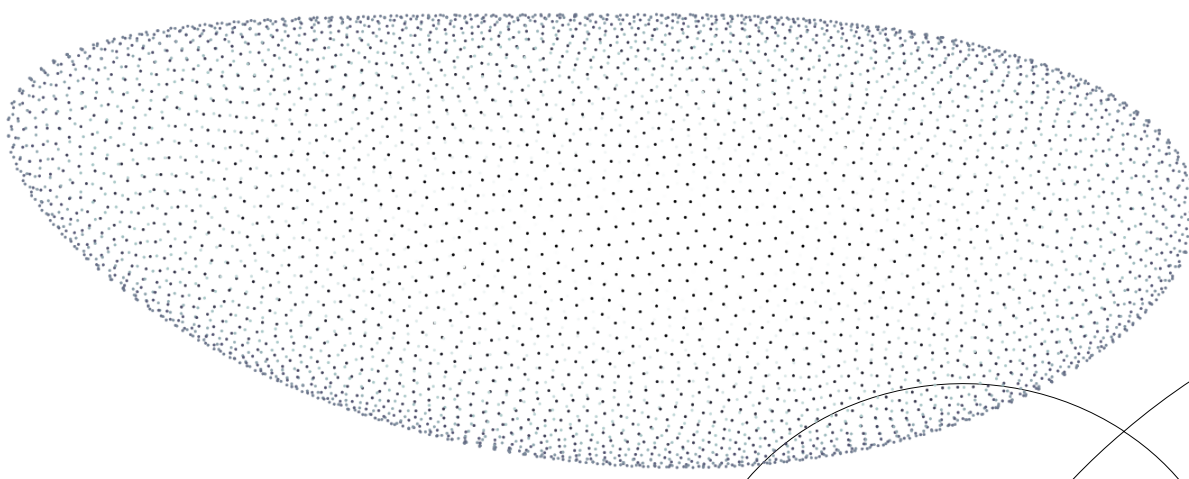


UNIVERSITY OF COPENHAGEN  
FACULTY OF SCIENCE  
NIELS BOHR INSTITUTE



## Master's Thesis

Jakob Hallundbæk Schausler

# Patterning and Emergence: **Drosophila Gastrulation In Silico**

Exploring morphogenesis from single-cell biophysics

Supervisor: Ala Trusina

October 2024

## Abstract

All biological systems involve intricate inter-cell coordination. Most of these cells use the same array of seemingly simple actions to achieve wildly different and complex results. This coordination needs to robust and precise to make multicellular life feasible.

In this thesis we explore how emergent phenomena at multiple scales help facilitate morphogenesis, the construction of physical shape. Focusing on fruit fly (*Drosophila melanogaster*) gastrulation, we propose a biologically founded, agent-based model with a minimal rule-set. Using gene expression data, we reduce full-embryo gastrulation to a few cell-level parameters. Through qualitative and quantitative analyses, the dynamics of the simulation are compared to what is observed *in vivo*, confirming overall alignment. Finally, we use the model to perturb known morphogenic events, observing how their complex interplay are vital in shaping the resulting animal.

## Acknowledgements

I would like to thank Arnulf for reading and giving notes ("It's better than House of Leaves"). I would also like to thank Daniel Alber for an interesting lab-tour, Teresa for helping me understand biology, Frederik for help in writing, Karoline for forcing me to keep writing, Christian Kragh Jespersen for lodging, and Sebastian for vital sparring throughout the project.

An finally a big thank you to Ala for a great trip to Princeton (and also supervision).

# Table of Contents

Abstract . . . . .	i
Acknowledgements . . . . .	ii
<b>1 Introduction</b>	<b>1</b>
<b>2 Theory</b>	<b>3</b>
2.1 Broken Symmetries & Genetic Patterning . . . . .	3
2.2 How Cells Move . . . . .	7
2.3 The <i>Drosophila</i> Gastrulation in detail . . . . .	10
2.4 Previous Attempts at Simulation . . . . .	13
2.5 The Model . . . . .	14
2.6 Implementation . . . . .	20
<b>3 Results</b>	<b>21</b>
3.1 Implementation . . . . .	22
3.2 Qualitative Agreement . . . . .	25
3.3 Quantitative Agreement . . . . .	40
3.4 In Silico Mutants . . . . .	50
<b>4 Conclusion</b>	<b>64</b>
<b>Bibliography</b>	<b>65</b>
<b>Appendix</b>	<b>69</b>

# Chapter 1

## Introduction

In 1952, two years before his untimely death, Alan Turing wrote an article called *The chemical basis of morphogenesis*.<sup>[32]</sup> In it, he predicted that the diffusion of off-equilibrium chemicals, combined with relatively simple interactions could originate much of the extraordinary patterning we see in nature. When talking about these chemicals, Turing coined the term morphogens, a merge between the greek words *morphe* and *genesis* – cementing them as facilitators for morphogenesis, the formation of physical form.

The fact that simple interactions between individual constituents can lead to complex and surprising behavior on a larger scale, (i.e. emergence), is one of the core concepts in physics. But just like no individual water molecule knows the shape of a wave, no single cell knows what a human is. All biological systems involve intricate inter-cell coordination, which needs to be robust and precise for multicellular life to be feasible. Most of these cells use the same array of seemingly simple actions to achieve wildly different and complex results. On top of this, Nature is remarkably consistent. Any two livers across organisms of the same species are functionally the same. The translation from blueprint to finished structure must either be very precisely controlled or innately exhibit strong error correction.

Takin our onset in the idea of emergence, we will be introducing a model that, through simulating the emergent behavior of individual cells, captures the large scale full-embryo movements that is seen in nature. We will be looking at morphogenesis in early stages of the fruit fly embryo. The common fruit fly (*Drosophila melongaster* among friends) has been studied for

decades and is used as a model for understanding many part of the earliest stages of life. Especially *gastrulation*, the point in which the inside- and outside domains are defined and separated has been studied intensively and has birthed multiple Nobel prizes. We will be highlighting three events during the approximate 15 minutes this gastrulation takes, and through simulation of these, we will be corroborating the validity of our model. By perturbing the model and seeing how the events independently and collectively react we will be showcasing the novelty, justification and value of our bottom-up approach.

How form arises, how cells coordinate, and how this can be modeled will be explored in the following chapters.

# Chapter 2

## Theory

To establish our model and its theoretical basis this section we will start by introducing some fundamental biological concepts, before specializing in the science of fruit fly gastrulation.

We will go through a wide, yet cursory explanation of the amount of information that is kept on cell- and embryo-level. Afterwards we will delve deeper into the fascinating biology that allows each cell to partake in the creation of a complex living animal. Finally, these concepts are all pieced together in the model that forms the basis of our research. Hopefully, by the end, every term and parameter should seem sensible and biophysically justified.

### 2.1 Broken Symmetries & Genetic Patterning

#### 2.1.1 Broken Symmetries

The interplay between order and symmetry is fundamental to any structured system. When a system develops complexity, it necessitates the breaking of an invariant, which arises from the disruption of symmetry.<sup>[2]</sup> Symmetry breaking occurs at all levels of biological development, where small-scale ordering influence and shape the global symmetries of the organism.

Every organism on this earth form in the same way: a single, fertilized cell suspended in a liquid. Through mitosis this single unit copies itself repeatedly, with each copy doing the same, ending in an isotropic sphere of cells. Suddenly, the cells will start moving in a coordinated manner, developing

the shape of the organism to come. However, as animals are not spherically symmetric, a number of symmetries need to be broken.

We will now go through some common examples to help elucidate how the different embryo-scale axes can be defined.

In *Drosophila*, after the first rounds of mitosis, the cells begin sensing a chemical gradient in the yolk towards the shell which allows them to migrate and line the inside of the egg. This allows each of their surfaces to form distinct "outside" and "inside" domains. Preferential adhesion comes into play here, where cells can selectively adhere to specific parts of their neighbours. Through preferential adhesion, based on their relative surface orientation, the cells can maintain their positions and the overall structure of the shell, even in the absence of external support. Thus our first symmetry break occurs, as this gives rise to the well defined embryo-scale inside-outside polarity. In biology this is known as **Apical-Basal polarity** which is observed in almost every multicellular system on the planet.

The second symmetry break is relates to the up/down-symmetry. This happens differently for different animals, but the most well known example is found in the frog *Xenopus*, where the rotation of the egg, relative to the point of sperm entry, establishes this axis. In ways like this, the belly and back (Dorsal-Ventral axis) can be defined. In the fruit fly, the up-down axis is defined from before fertilization through asymmetries in the egg.

Finally, we need some way of getting every cell to know an in-plane "forward" and "backward" direction. This polarity is called **Planar-Cell Polarity** (PCP) and is almost as ubiquitous as the Apical-Basal polarity. In *Drosophila*, PCP is defined by morphogen gradients giving a clear (nematic) in-plane direction, perpendicular to the inside-outside (AB) polarity. As defined in the introduction, morphogens, as predicted by Turing, are signaling molecules that help establish these asymmetries. These morphogens have distinct and stable patterning of low and high concentrations which the cells can sense and react to.

The next step is to understand how these patterns emerge and how they lead to coordinated development across the embryo:

### 2.1.2 Genetic Patterning

For a multicellular organism to go from a homogeneous cell sheet to forming complex body plans, quite a bit of self-organizing is needed. The complicated interplay between cells necessitates both large-scale and cell-scale control. For human and fruit fly alike, this is done via genetic patterning.[33] As predicted by Turing, patterning is a result of "smartly"<sup>1</sup> designed interactions where different chemicals assist or inhibit the production or expression of each other. These concentration gradients are both precise and robust enough to be picked up by the individual cells which allows for independent differentiation on a cell-by-cell basis.

To get a feel for the amazingly complicated and remarkably precise patterning of these chemicals, four of them can be seen in Figure 2.1 below:

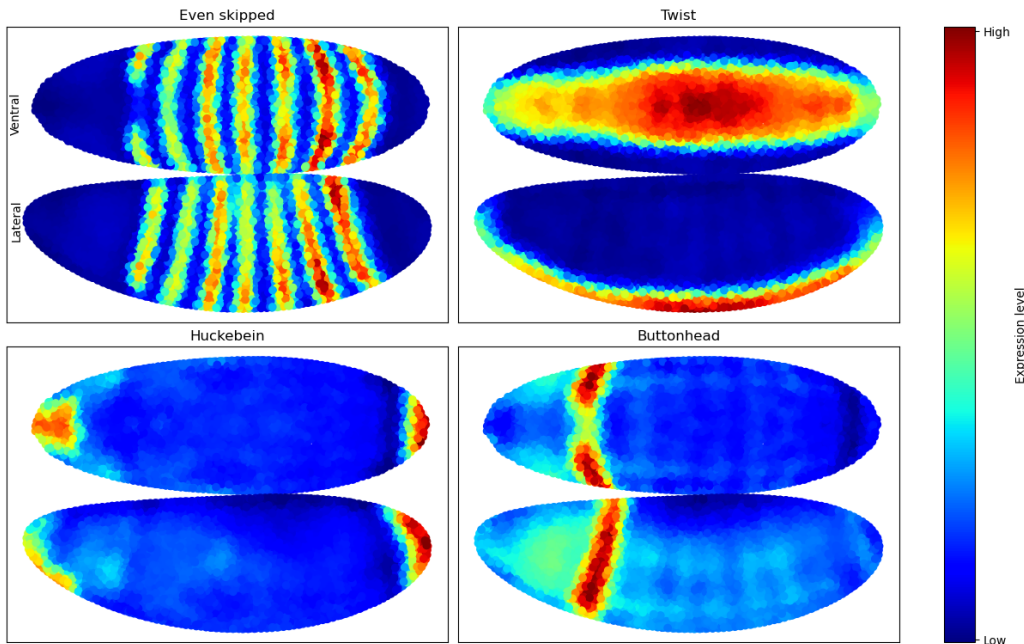


**Figure 2.1:** The spacial distribution of a small subset of morphogens; a clear attest to the remarkable and stable pattern formation Turing predicted simple interactions between chemicals gradients capable of producing.

---

<sup>1</sup>Nature abhors a vacuous anthropomorphization

The cells in an embryo can, using internal mechanisms, react to their local concentration of these chemicals, allowing them to act accordingly. These local reactions can consist of everything from simple mechanical activity in the cell walls to changing its internal composition:

Each cell maintains its own distribution of these chemical gradients, providing a second, local basis for directed responses and collective organization. These individual gradients are intrinsically connected to the polarizations discussed in the last section, and play a big role, both in natural processes and in the model we will be introducing later. In the next section the different biomechanical actions the cells are capable of will be discussed, but first we will have to understand how signaling and mechanical changes interact.

The link between morphogens and mechanical deformations go both ways. This means, that when cells move according to some defined polarity, they can move the signal with them and break the symmetries of other other cells along the way. It has been shown that a mechanical stimulus can trigger a chemical signal, thereby re-inducing patterning in a feedback loop. This is called **mechanotransduction** and is vital in stable morphogenesis[4]. A relevant example of mechanotransduction is how cells can sense movement from a particular direction and respond by aligning their *Planar-Cell Polarity* accordingly.[12] This local alignment can trigger a cascading effect, ultimately contributing to the overall shape of the tissue.

Let us take a small step back and think how extraordinary this all is. Every individual action is transcribed from the same string of DNA, where nothing happens except building one of 20-ish amino acids to form proteins. These proteins can then either help or delay the transcription of the same DNA string. It is the order in which these simple proteins are created that, together with the relatively simple physical self-interaction, allows for the exponentially more complex cell to emerge.

And now, the same thing happens on the next level: Individual cells will each be making simple mechanical alterations to their shape. The interplay between these can somehow arrive at a cohesive bigger picture. To understand this behavior, we will need to look at the individual mechanisms:

## 2.2 How Cells Move

Most of the global, large-scale motion seen during development of any multi-cellular organisms stem from a handful of seemingly simple – albeit still not well understood, active, single-cell actions.[34]

In many cases, cell migration consist of *chemotaxis*. That is, individual cells moving in the direction of a chemical gradient.

What we will be looking at is fundamentally different. In embryogenesis, where cells are closely bound together in epithelial sheets, the cells are able to exert forces on *each other*. As can be seen on Figure 2.2, the cells stay interconnected using membrane tethers connecting local neighborhoods. This means every cell can change its shape relative to its bordering cells allowing for combined motion more efficient than any single cell could achieve on their own.[26]

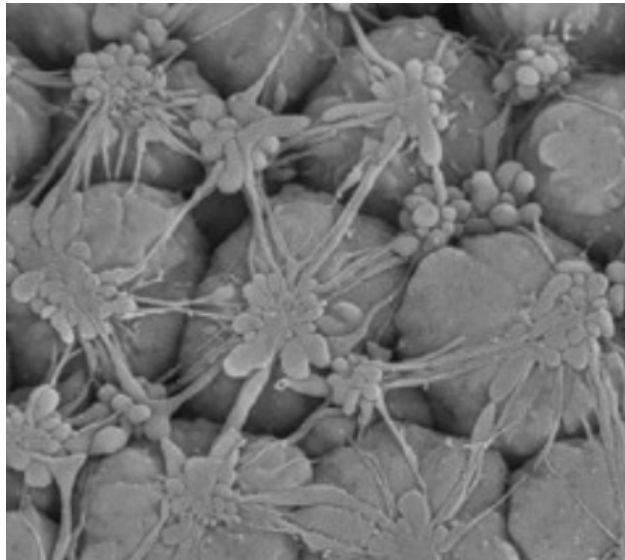


**Figure 2.2:** Electron microscopy of *Myosin II*-protein meshwork on the belly-side of the fruit fly embryo. (Source: Martin et al. (2010))

Studying these **local motions with global consequences** is the main point of focus for us. Unfortunately experimenting with living cells is inherently hard, which means that in fruit fly gastrulation, the driving effects are surprisingly poorly understood with no paper claiming to have an exhaustive

list. Here are some of the fundamental single-cell active forces that undeniably are affecting the gastrulation: **Convergent Extension** and **Apical Constriction**

### 2.2.1 Convergent Extension

For elongating sheets of tissue, *Convergent Extension* is one of the most common driving forces. It is made up of asymmetric cellular intercalations. In layman's terms: Cells moving in between each other, like the teeth on a zipper. In Figure 2.3a a schematic of how cell intercalation can lead to extension is seen.

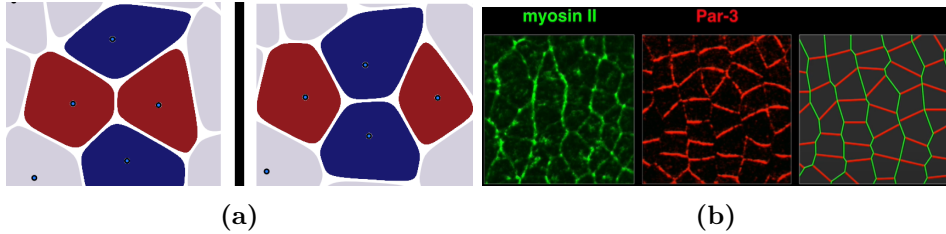


**Figure 2.3:**

- (a): A diagram showing how guided intercalation of the blue cells in the vertical direction can result in horizontal elongation of the cluster.
- (b): Dyed germ-band tissue showing a clear difference in horizontal and vertical protein expressions (Source: Zallen and Wieschaus (2004)) The individual cells can utilize this anisotropy to direct their intercalation.

The Planar-Cell polarity, as described in the previous section, can give rise to a stark difference of protein concentrations between horizontal and vertical cell walls. This can be seen in Figure 2.3b. Through anisotropic tightening of cell borders, with deformations only happening in the individual cell, the full sheet can change shape. No cell even needs to know its position in space or barely change its shape.

This contraction on a specific side of a cell, leads us to the next fundamental active force.

### 2.2.2 Apical Constriction

When the cell sheet wants out-of-plane bending, they turn to *Apical Constriction*. As the name suggests, protein rings constrict the apical (outer)

side of the cell, creating a smaller surface area on one side. This leads to bending and, when enough constriction is applied, invagination. (see Figure 2.4). Cells have shown the ability to constrict both isotropically and anisotropically (relative to the Planar-cell Polarity) granting cell-sheets the ability to form both valleys and cavities.

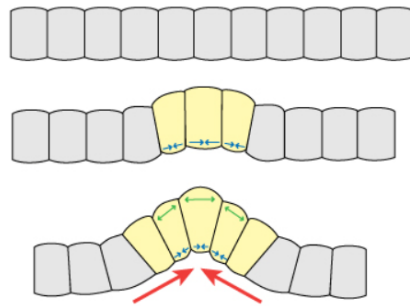


**Figure 2.4:** Schematic for how apical constriction works. A number of cells mechanically lower their surface area on their outer (apical) side resulting in a large-scale invagination when pressure is applied.

Now, the fact that nature is thrifty with its creations, means that versions of the few actions described above are used in the creation of almost every type of organ in almost every type of organism. The hope is, that understanding these fundamentals in one system might allow for lessons to be learned in another. In this thesis we will focus on the motility required for *Drosophila* gastrulation to arise. As explained in the introduction, the fruit fly is a model organism, and the fact that it has been observed by biologists for years makes it a great subject for probing the intricacies of biomechanics.

To summarize what we have learned: Through *genetic patterning* and other *broken symmetries* both the embryo on the whole, and each each cell, contain off-equilibrium protein densities, and, through the distribution of these, well-defined *polarities*. Through *mechanotransduction*, *local movements* can be tied to these polarities and vice versa, allowing for stable, global morphological changes to occur. Examples of these local driving forces are *convergent extension* and *apical constriction*.

## 2.3 The *Drosophila* Gastrulation in detail

In the literature, the development of the fruit fly from fertilised egg to hatched larvae is usually divided into 17 distinct events.<sup>[5]</sup> We will be looking at stages 5 through 7. These are characterized by having the first mesoscopic, morphogenic movements and setting the stage for all the action to come.

But first, a quick rundown of the first 5 stages: The *Drosophila* egg has an oblong shape with a diameter of about 1/10th millimeter.<sup>2</sup> Rather than immediately dividing into separate cells, the fertilized egg first undergoes several rounds of nuclear division within one large cell. This unique arrangement results in about 5000 nuclei lining the shell of the egg. Eventually, each nucleus becomes encased in its own membrane, marking the *cellular blastoderm stage*, where distinct cells finally emerge.

These cells now start an event lasting about 15 minutes. This step, called the *gastrulation*, consist of a series of interconnected but independent cell movements. These local motions lead to global, temporally evolving morphological changes defining the inside- and outside layers of the fly.

We will now present an abridged overview of the gastrulation, roughly ordered in time. In it, three events have been highlighted, chosen for being both instrumental for the final morphological outcome and relating to spatially different domains of the embryo.

---

<sup>2</sup>Source: This wonderful website: <https://bionumbers.hms.harvard.edu/bionumber.aspx?id=111360>

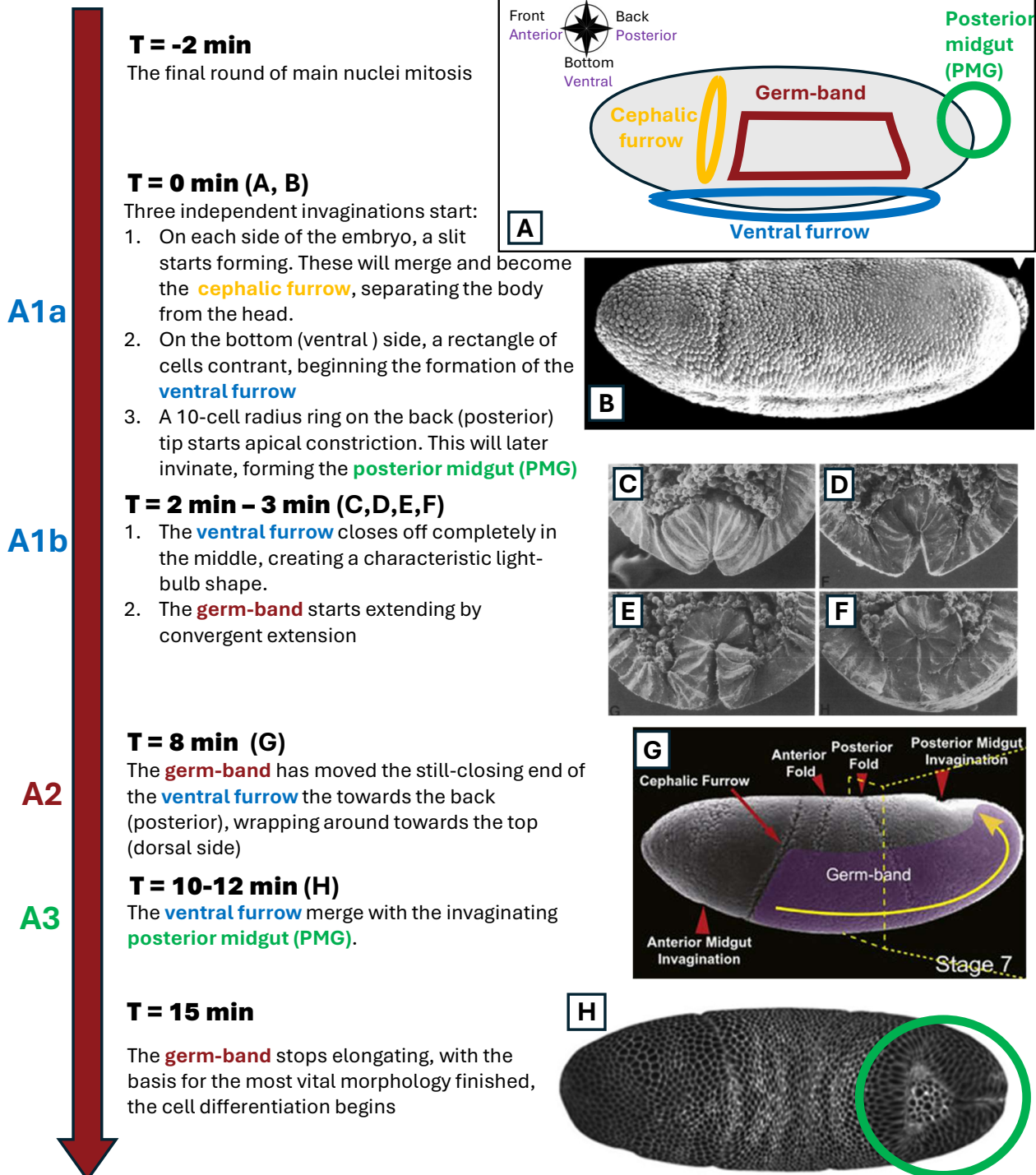


**Figure 2.5:** (*Previous page.*)

A somewhat comprehensive explanations of the most important parts of the early *Drosophila* gastrulation. The three events (**A1**, **A2** and **A3**) have been highlighted by us for later referencing.

**A:** A diagram of the *Drosophila* embryo as it is usually depicted: The front side (what will become the head) facing left. The primary domains of interest are depicted.

**B:** An electron microscope image of the embryo around 30 seconds after initialized gastrulation. The early signs of the cephalic furrow and ventral furrow are visible. On the anterior (back) tip, a number of germ cells (called pole cells) can be seen.

**C - F:** Electron microscopy of a cross section of the ventral furrow closing off (**A1**). (Source: [Sweeton et al. \(1991\)](#))

**G:** A diagram of the motion of the germ-band as it extends (**A2**). The locations of auxiliary folds are also highlighted. (Source: [Kong et al. \(2017\)](#))

**H:** Imaging of the embryo with highlighted cell walls. We can see the posterior midgut as it invaginates and combines with the ventral furrow (**A3**). (Source: [Stern et al. \(2022\)](#))

A video of the gastrulation can be found [here](#).

As we now have the basis for understanding in place, we can pose our main questions succinctly:

We would like to see, with as few parameters as possible, how close we can get to the gastrulation seen *in vivo*. Here we will focusing on the three main events (**A1**, **A2** and **A3**) as described above.

Secondly we would like to see whether any explicit timing-dependence is needed for the quite temporally complex chain of events to unfold.

Finally, given a model we are have confident in, we would like to probe it about the interplay between its different spacial domains. Specifically, how removing any of the above events affects the progression of the others.

## 2.4 Previous Attempts at Simulation

In silico models has provided multiple working examples of all the aforementioned embryogenetic events with multiple different approaches since the 1970's. Much of this section will draw from the review [Loerke and Blankenship \(2020\)](#) which complied an overview of the different state-of-the-art methodologies and results.

When studying the biomechanics of morphogenesis there seems to be two primary strategies:

**Isolated Active Event:** This strategy focuses on a single morphogenetic event, modeling it in detail. For instance, ventral furrow formation ([A1](#)) can be simulated as an elastic sheet subjected to pulling forces. This approach can enhance our understanding of the physical forces or biological mechanics required for an event to occur but may limit generalization to other morphogenetic processes.

**Isolated Active Phenomenon:** In this approach, a single active phenomenon, such as convergent extension (the driving force in [A2](#)), is simulated "in a vacuum." This allows for a detailed comparison of the actions of individual cells against imaging. This method can provide great insight into the underlying physics and chemistry in the cells, but falls short in shedding light on any specific activities, especially as it omits influence from any outside context.

Our approach will fall in between the two above, in previously unexplored territory; simulating everything, everywhere on the embryo, all at once. But to understand how this is feasible (and the inherent drawbacks and simplifications), we will need more context.

Vertex-based and continuum approximation-based simulations have dominated the field since computer modeling of biology started. These are great for accurately describing the minute changes in the physics of tubologenesis, tissue-folding etc., but they come with some inherent downsides. These models focus on the pressure and tensile forces, simulating the strains in the cell walls and looking at sub-parts of cells are often computationally heavy. This requires it to be done in 2D[[17](#)], inherently loosing some particularities

of the problem.

A more computationally efficient approach is the cell-center based models. For cell-based models, doing the computation on a lattice is by far the most prevalent method, again gaining speed by trading particularities of the problem.

When looking for off-lattice, center-based model, not many show up. An example is Atwell et al. (2015) who simulated tube extension by mitosis, but only using non-polar interactions. Looking for full embryo *Drosophila* models, the highlight is Allena et al. (2010) where they simulate the same three events we will be focusing on, but only individually.

This all boils down to: No one has been able to successfully simulate the formation of the posterior midgut (**A3**), as this requires a successful model of the ventral furrow (**A1**), germ-band extension (**A2**), and a way to combine them, necessitating a simulation of the full embryo with multiple different types of interactions.

## 2.5 The Model

Our model takes its onset in the ideas posed in Nissen et al. (2018), later expanded in Nielsen et al. (2020). Whenever we deviate from the existing literature, this will be stated clearly.

As we know global changes in physical structure during gastrulation all arise from single cell actions with little discernible individual movement. Our model is built around simulating the cells as point-based particles, elevating their internal chemical gradients to vectors with explicitly stated orientations. It is based on the following intercellular potential  $V_{ij}$  described by:

$$V_{ij} = e^{-r_{ij}} - A_{ij}e^{-r_{ij}/\beta} \quad (2.1)$$

Where  $r_{ij}$  is the (unitless) distance between two cells,  $A_{ij}$  is an attraction factor that will be explained later, and  $\beta$  is a constant that sets the scale between these two. The first term is a short range repulsion preventing them from overlapping and the second is a long range attraction defining

their interactions. The constant  $\beta$  (usually set to 5, which is very constant) effectively defines the cell size for a given  $A_{ij}$ .

Now, every individual cell  $i$  tries to minimize the quantity

$$U_i = \sum_j V_{ij} \quad (2.2)$$

where the sum over  $j$  is over all line of sight/Voronoi neighbors. Voronoi neighbors are cells that share a boundary in a Voronoi diagram (see Figure 2.6).

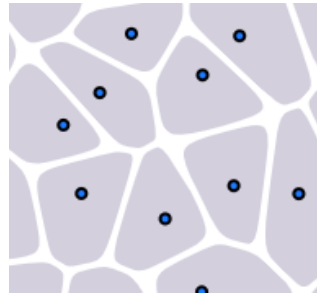


**Figure 2.6:** A Voronoi diagram. Every point within a region is closer to its respective *cell* than to any other *cell* in the space. The regions are drawn with rounded corner for no other reason than to mimic biology.

To get a feeling for  $V_{ij}$  (Equation 2.1), the potential can be seen in Figure 2.7 for  $A_{ij} = 1$ .

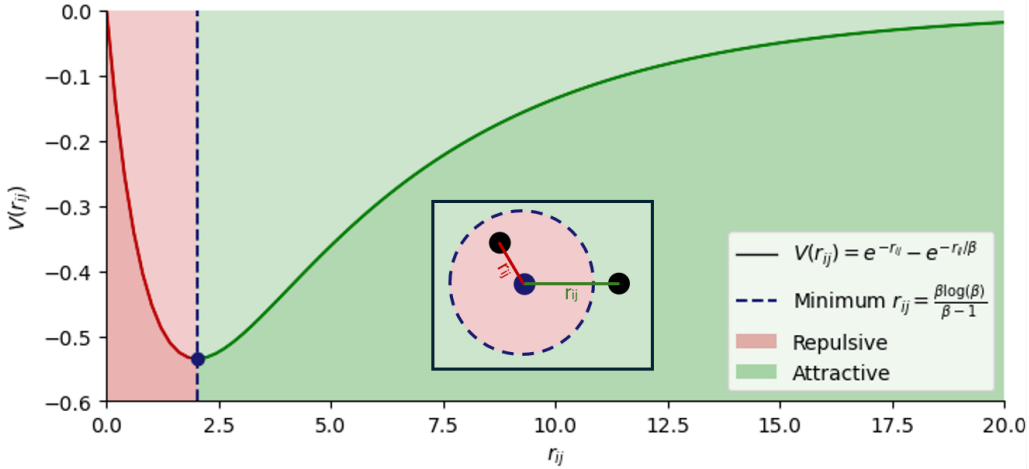


**Figure 2.7:** The potential as defined in Equation 2.1 for a single particle and neighbor, with the minimum (i.e. effective cell size) drawn in. On the inset axis an example of a cell with two neighbors, one with a distance that would result in a repulsive force and one attractive. Here we also see the role of  $\beta$  as responsible for regulating the relaxation-distance.

The shape of the potential well should remind you of the Yukawa/Lennard-Jones potential, which also rely on strong short-range repulsion and weaker, longer-ranged attraction.

Running the simulation at this point, the cells would simply converge to a packed sphere, much like the earliest stage of the *Drosophila* embryo.

Now, just like in nature, some symmetries needs to be broken to allow for interesting morphologies to emerge.

As explained in the last section, internal protein aggregates allow each cell to have their own polarizations. Through mechanotransduction and nearest-neighbor interactions, these polarizations can shape the cell and vice-versa. The idea is now to elevate the Apical-Basal and Planar-Cell polarities (as described previously) by seeing them as explicitly stated polarization vectors with rules for intra- and inter-cell interactions.

The first symmetry that is broken is the inside-outside symmetry. Introducing the (normalized)  $\hat{p}$  vector for each cell allows for emulation of the *Apical-Basal* polarity. This motivates the following term which I will explain

after introducing:

$$S_1 = (\hat{p}_i \times \hat{r}_{ij}) \cdot (\hat{p}_j \times \hat{r}_{ij})$$

$S_1$  ties the relative positions between a cell and its neighbors  $\hat{r}_{ij}$  to their respective AB-polarities  $\hat{p}$ . As can be seen, this is a dot-product of cross products. This configuration can be understood for  $(a \times b) \cdot (c \times d)$  as "keep a and c, and b and d respectively parallel, while keeping a and b, and c and d internally perpendicular".<sup>3</sup>

In the case of  $S_1$ , it encourages cells to lie in a plane, perpendicular to their AB-polarities. A diagram of the effects can be seen below (Figure 2.8). Adding the  $S_1$ -term to our potential produces sheets of cells.

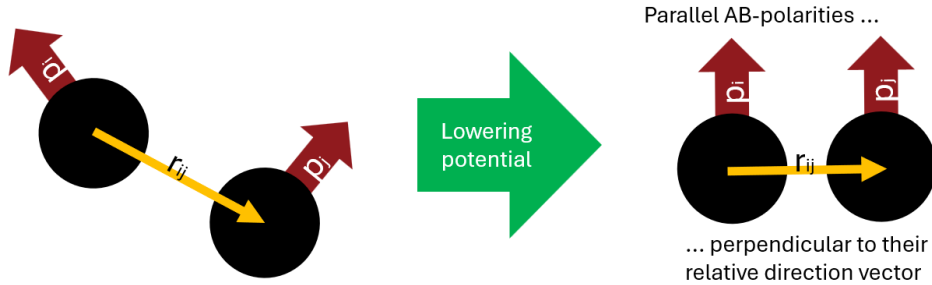


**Figure 2.8:** A visualization of the effects of the  $S_1$ -term.

The second symmetry break is the planar polarization. We introduce the Planar-Cell-Polarities  $\hat{q}$  (PCP from here on), and define the dynamics as follows:

$$S_2 = (\hat{p}_i \times \hat{q}_i) \cdot (\hat{p}_j \times \hat{q}_j)$$

This term keeps the PCP and AB polarities perpendicular within each cell, but aligned across cells. This gives a stable and consistent, but changeable in-plane orientation vector for each cell. A diagram can be seen in Figure 2.9. Importantly, the  $\hat{p}_i$ 's and  $\hat{q}_i$ 's are unit vectors and are therefore constrained to being normalized.

---

<sup>3</sup>This can be shown by, using some cross-product identities, changing the expression to a sum of dot-products. This has been left as an exercise for the censor.

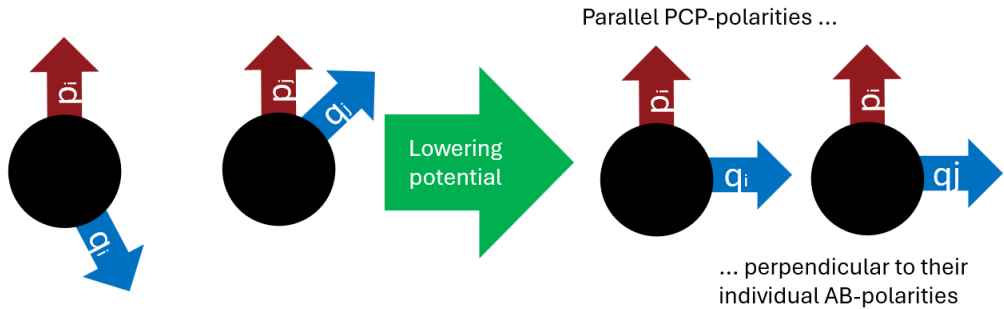


**Figure 2.9:** A visualization of the effects of the  $S_2$ -term.

To take advantage of this well-defined direction of motion, we will take inspiration from the Convergent Extension (Section 2.2.1) and introduce the final step of the dynamics, coupling the cells relative positions with their PCP-vectors.

$$S_3 = (\hat{q}_i \times \hat{r}_{ij}) \cdot (\hat{q}_j \times \hat{r}_{ij})$$

This term is lowest when the Planar-Cell-polarities are aligned but perpendicular to their relative direction-vector. In the realm where this term dominates, the cell sheets created by  $S_1$  and  $S_2$  are exchanged for lines of cells perpendicular to their PCP-vectors. Below (Figure 2.10) the effects are represented graphically.

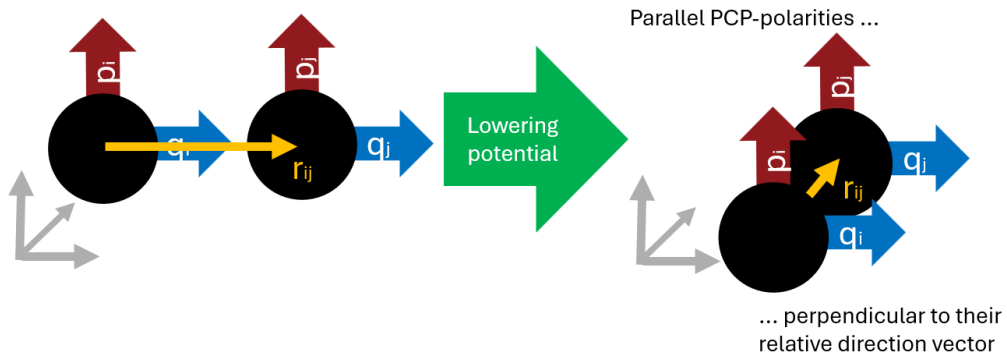


**Figure 2.10:** A visualization of the effects of the  $S_3$ -term.

While the mechanics are not capturing the explicit deformations that drive convergent extension, this term allows for directed cell intercalation.

The full array is therefore:

$$S_0 = 1 \quad (2.3a)$$

$$S_1 = (\hat{p}_i \times \hat{r}_{ij}) \cdot (\hat{p}_j \times \hat{r}_{ij}) \quad (2.3b)$$

$$S_2 = (\hat{p}_i \times \hat{q}_i) \cdot (\hat{p}_j \times \hat{q}_j) \quad (2.3c)$$

$$S_3 = (\hat{q}_i \times \hat{r}_{ij}) \cdot (\hat{q}_j \times \hat{r}_{ij}) \quad (2.3d)$$

We can now finally introduce the more complicated  $A_{ij}$ -parameter as teased in Equation 2.1. We see it as a sum of the four previously described  $S_i$ -terms, each with an associated scaling factor  $\lambda_i$  for

$$A_{ij} = \sum_{n=1}^3 \lambda_n S_n(r_{ij}, p_i, p_j, q_i, q_j) \quad (2.4)$$

If the constraint  $\sum_{n=1}^3 \lambda_n = 1$  is not fulfilled, the relaxed cell size is not constant.

Adding to our array of actions the cells can take, we introduce the second mechanical activity described earlier: Apical constriction (Section 2.2.2). In our model, this is done via **Wedging**

As apical constriction us a way, for a single cell to create large-scale furrows, we implement this by changing the  $\hat{p}_i$ 's to 'trick' each cell into believing their neighbors are differently oriented, thereby changing the relaxation angle:

$$\tilde{p}_i = \frac{\hat{p}_i - \alpha \hat{r}_{ij}}{|\hat{p}_i - \alpha \hat{r}_{ij}|} \quad (2.5)$$

A similar expression can be made for anisotropic wedging, taking the in-plane  $\hat{q}_i$ 's into account.

All cells can now be defined by a cell type, which simply means they have a  $\lambda$ -array and an  $\alpha$  associated with them.

## 2.6 Implementation

As we estimate the cells to move slowly and in a friction-filled and viscous yolk (the low Reynolds number-regime), each time step the cells move as subjects to overdamped dynamics. For a cells position  $r$  and the two polarization vectors:

$$\frac{d\bar{x}_i}{dt} = -\frac{dU_i}{d\bar{x}_i} + \eta \quad | \quad \bar{x} \in \{\bar{r}, \bar{p}, \bar{q}\} \quad (2.6)$$

where  $\eta$  is uncorrelated Gaussian noise and  $U$  is the total potential as defined in Equation 2.2.

The gradient is calculated via an automatic differentiation engine (The PyTorch-framework specifically) and the simulation time steps are calculated via Euler integration.

Every frame, the positions, AB-vectors and PCP-vectors are saved. As the model is purely point-based, whenever we speak of inter-cellular junctions, neighbors, areas or angles, everything is inferred from the modeled point cloud and Voronoi-neighbors.

The computer science is not the interesting part of this thesis, so notes on the actual implementation along with pseudocode can be found in Section A4 in the Appendix.

# Chapter 3

## Results

After building up intuition on the biological features of a *Drosophila* embryo and a model capable of (somewhat crudely) mimicking it, we can now begin probing our model for interesting phenomena. We know that cells in nature act by relatively simple, local rules. Having added a small number of these to our model, we would like to see whether it can emulate gastrulation reminiscent of what is seen *in vivo*. Focusing not just on the final structures, but also all the pivotal events leading up to it.

Once we have assessed the phenomenological validity of our model, we will look onward for intriguing phenomena to study. Given our full-embryo model, we will be looking into the interplay between the different active domains and events.

On the structure: We will start out by defining the problem-specific additions and our found parameters of the model. Following that, we will go through the similarities between simulation and reality, starting from simple visual comparisons, ending in detailed quantifications. We will do these for the different events ([A1](#), [A2](#) and [A3](#)) and embryo domains. Afterwards, we will be looking at removing different active parts of the simulated embryo, comparing the results to known real-life mutants. This will finally lead us to a purely *in silico* analysis of the interaction between spatially distinct domains of the embryo.

### 3.1 Implementation

We will now be diverging from the original papers, and update the model for our specific case:

As the shape of the egg shell is proposed to be defining for the gastrulation, **boundary conditions** are parameterized by hand from visual references and added as an exponential term to the potential.

A slight **differential adhesion** was added to simulation. This covers the concept that some cell types have preferences (encouraging or discouraging) about which other cell types to adhere to. The interaction between the ventral furrow cells (cell type 2) and cells of other types were scaled by a factor of 5% (multiplied by 0.95) so as to discourage unnecessary mixing.

To emulate the lowering of apical surface area **better emulation of apical constriction** was introduced. Invaginating cells ( $\alpha > 0$ ) got an increase in their  $\lambda_1$ 's (in Equation 2.3b) making their relaxation distance shorter. This had the added benefit of echoing the tighter bonds in constricting cell clusters.

We removed penalization for "outside-touching-outside", i.e. two **apical sides touching**. When any of the invaginating tissue 'closed off' it forced cells on either side to have their AB-vectors pointing towards each other. This would get penalized in their  $S_1$ -terms (Equation 2.3b) making any folds unstable. To combat this the model was changed, so when two outer sides (apical sides) interacted, they were only allowed to interact non-polar'ly, i.e. their  $\lambda_1$ -values were changed into  $\lambda_0$ .

Taking inspiration from Kirkegaard et al. (2019), a **nematic planar-cell polarity** were implemented. This was mainly done so as to better mimic natural in-cell gradients. This means changing the definition of  $A_{ij}$  in the following way:

$$\begin{aligned} A_{ij} &= \sum_{n=0}^3 \lambda_n S_n \\ &\downarrow \\ A_{ij} &= \lambda_0 S_0 + \lambda_1 S_1 + \lambda_2 |S_2| + \lambda_3 |S_3| \end{aligned}$$

And finally, the most important contribution – **patterning**:

As we have about 5000 cells with four  $\lambda$ 's and a wedging constant  $\alpha$  for each, this effectively gives 25000 parameters. To combat this, we again look to nature and remember the patterning Section 2.1.2. Somehow all the information a cell needs can be found available in these initial conditions.

In Karaïkos et al. (2017) they map out the relative gene expression for the *Drosophila* embryo. We can then take this spatial data, project it onto our embryo and cross reference with known molecular activators of developmental processes. This approach enables us to identify specific cell types based on their gene expression profiles and their corresponding roles in key morphogenetic events. Our model will still run 'bottom-up', with all necessary conditions initialized before the simulation, but by cross-referencing in this way, we establish a pipeline that connects morphogen gradients to the morphogenesis. This not only enhances our simulation by justifying cell roles, but might also shed some light on how the spatial patterning of gene expression orchestrates the choreography of embryogenesis.

Having established the pipeline, a demonstration of how to define the initial conditions can be seen here:

```
# Start a new egg from a relaxed base shape
GE = GeneExpression("path/to/base_shape")

# combine morphogens through [and, or, not]
twist_and_snail = GE.and_gene(GE.gene("twi"), GE.gene("sna"))

# Make a cut-off (50%) in concentration and define cells as
#   belonging to a cell type (2)
GE.add_expression(twist_and_snail, 0.5, 2)

# save and run simulation
GE.save("name_of_expression_profile",)
```

Given 5 different cell types and no non-polar interaction, we have cut our parameter space down from 25000 to 20. An overview can be seen below (and in Section A8 in the Appendix the exact choices, justifications and additional notes can be seen):

Cell type	Genetic expression	Location	$\lambda_1$	$\lambda_2$	$\lambda_3$	$\alpha$
0	None	All non-active tissue	0.4	0.4	0	0
1	Eve & Runt	Germ-band ( <b>A2</b> )	0.4	0.4	0.08	0
2	Twist & Snail	Ventral ( <b>A1</b> )	0.8	0.4	0.04	0.2
3	Huckebein	Posterior ( <b>A3</b> )	0.8	0.4	0	0.2
4	Multiple	Auxiliary folds	0.8	0.4	0	0.5

We now have a working model!

A video of the final simulation can be found at the following link:

[Here](#)

## 3.2 Qualitative Agreement

While the *Drosophila* embryo has been studied for decades, it is only relatively recently that microscopy and computer science has gotten to a point where quantitative analyses of the more than 5000 cells have become feasible. Therefore, like in most of the fields history, we will start with visually examining the morphology of the embryo.

For all figures in this paper, if nothing else is noted, the run is the one named `finale`. In vivo, the time of invagination of the posterior midgut (**A3** in the overview) is about 12 minutes after start, the timing of the simulation is defined to align with this event, allowing for direct comparisons in "minutes" across simulated and experimental timelines.

We will start out this section with an overview which we compare to imaged embryos to ensure that there is general phenomenological agreement. We will then go through the individual main morphological events (**A1**, **A2** and **A3** from Figure 2.5) and qualitatively assess the resemblance between the simulated events and real embryos, hopefully providing some preliminary insight into the simulated mechanics. Finally, we will make some additional visual annotations to aid in estimating the nature of the tissue movements, which will help facilitating a more intuitive understanding of these developmental changes.

On the following page, we compare our best in silico model and corresponding frames from a imaging by Stern et al. (2022).

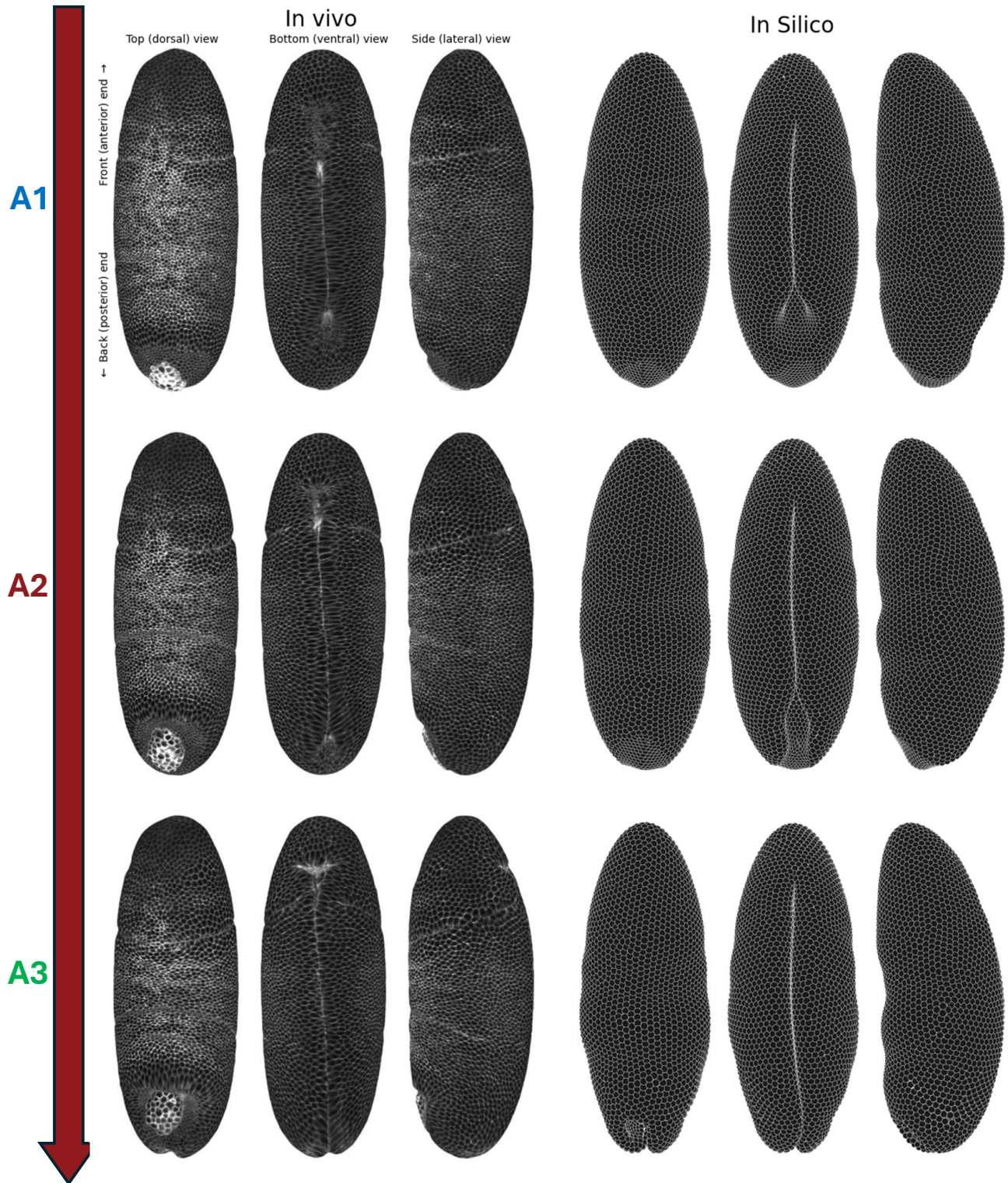


**Figure 3.1:** (Previous page.)

A full page visualization of three time steps of the simulation and corresponding point from in vivo imaging. Each row consists of a single time-step and corresponds roughly to the three previously highlighted primary events ([A1](#), [A2](#) and [A3](#)). Within each row, the embryo is shown from the top (dorsally), bottom (ventrally), and side (laterally), with the back end (posterior) pointing downwards. A cursory comparison reveals a general alignment in the overall morphologies.

**Left:** In vivo imaging with cell walls highlighted by use of a membrane marker (Source: [Stern et al. \(2022\)](#)).

**Right:** In silico visualization. For ease of comparison the colors have been made to match the data.

It is easy to hide behind numbers and advanced analytical methods, so for completeness sake we have started by presenting a visually unaltered full-scale comparison. Our analyses will soon be more sophisticated, but from a naive inspection, the general dynamics, timing and shape seems to generally have been recapitulated. Given the relatively simple model and few specific alterations, this is already notable!

But to understand the agreements between data and simulation we will need to scrutinize the individual pieces using some visual aids. Using the main events ([A1](#), [A2](#), [A3](#)) as starting points, we will go to a higher level of resolution, focusing on individual parts of the embryo, validating the simulation and comparing them to in-vivo imaging when available.

### 3.2.1 ([A1](#)) Ventral Furrow

The first sign of movement on the embryo is on the belly where a distinct cleft begins forming.

This is called the **ventral furrow** and is an important part of creating the gastrointestinal tract.

From Figure 3.1 we have from an external perspective seen the characteristic cleft form on the bottom side, mirroring the initial stages of invagination. The furrow closes off in just over three minutes.[\[13\]](#) As the furrow closes, the internalized cells form a tube with a recognizable light bulb-shape in the cross section.

Below, in Figure 3.2, a comparison between a cross section of our simulation and in vivo imaging can be seen.

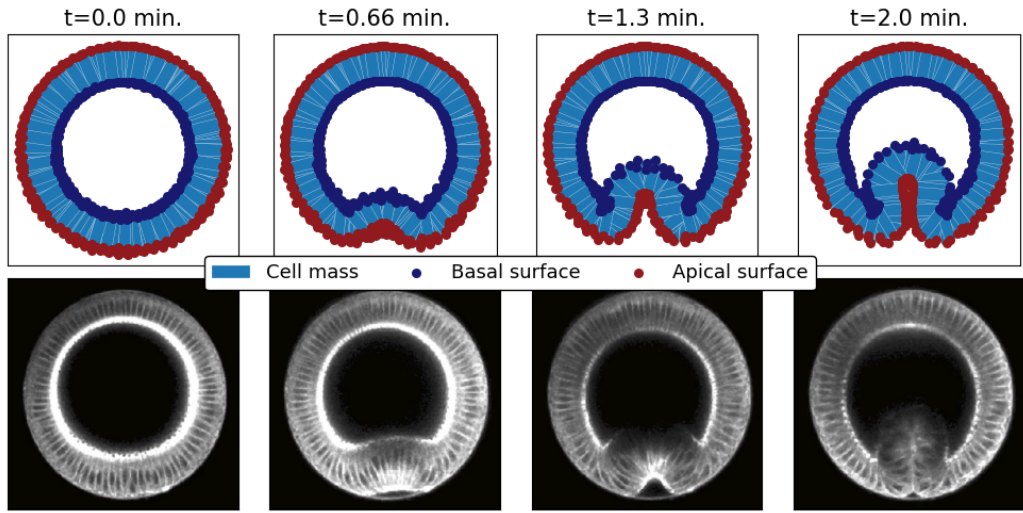


**Figure 3.2:** A comparison of cross sections showing the dynamic morphology of the ventral furrow formation (**A1**) in simulation (**upper row** and frames from video of live growth (**lower row**). For ease of comparison, each cell in the simulation is displayed as a rectangle with the longer side aligning with its simulated apical-basal-axis. The blue and red dots are approximations of the inner and outer cell walls, also calculated using their apical-basal polarities. The cutting plane used in simulation can be seen in Figure 3.3. The video is multi-photon microscopy of cell walls (Source: Conte et al. (2012))

Overall, both the motion observed during development and the final shape of the structure appear to be well aligned with the in-vivo observations.

In simulation, we can visually observe the same dynamic process of ventral furrow formation, with remarkable parallels to what occurs in the embryo (**A1**). In Figure 3.2 we can now see, that as the simulation progresses, the closure of the furrow and internalization of cells produce the familiar tube-like structure, with the cross-section displaying the previously mentioned light bulb-shaped profile. Adding to this, the directions of movement and rotation of apical- and basal sides of each cell closely match what is observed in real embryos, further validating its accuracy.

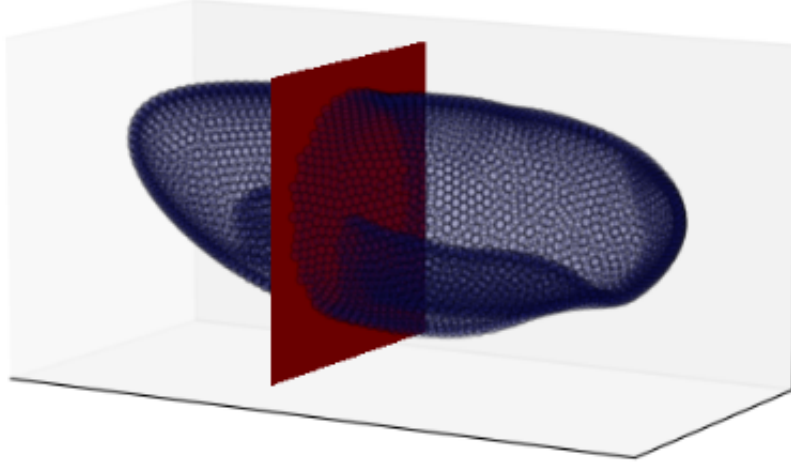


**Figure 3.3:** The cutting plane used for visualization in Figure 3.2 visualized.

In our simulation, the invaginating tissue extends slightly more towards the center. This is especially noticeable closer to the head (anterior tip) (see Section A3 in the Appendix). This problem also plagues the state of the art [Allena et al. \(2010\)](#) who did a full vertex-based simulation focusing on the ventral furrow. This common difficulty might stem from the fact that after closing, the ventral furrow starts 'pinching off' disconnecting the internalized cells which includes some dynamics not present in the simulations.[\[30\]](#) In general, we find the first key morphogenetic event ([A1](#)) – the formation of the ventral furrow – to have been adequately recreated.

### 3.2.2 ([A2](#)) Germ-band

The most numerous cell group we are interested in is the **germ-band** which fill most of the lateral sides. As mentioned in Section 2.2.1, it is generally agreed that the germ-band is one of the main drivers of horizontal motion, although it remains disputed how.[\[9\]](#)

In Figure 3.4 a text-book diagram of the motion of the germ-band can be compared with the shape of the germ-band in the first and last frame of our simulation.

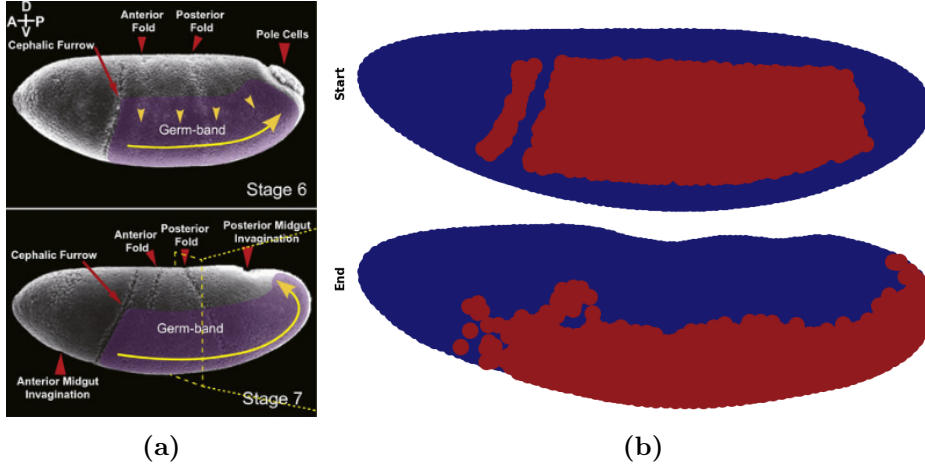


**Figure 3.4:**

(a) A diagram of the germ-band (purple shaded area) and its motion when extending (A2) (Source: Kong et al. (2017))

(b) Simulation with colored in germ-band at  $t = 0$  min and  $t \approx 15$  min

Note: The blue line separating the germ-band in the initial frame is a quirk of the gene-expression-cutoff as described in Section A8.

To reiterate, during gastrulation, the motion of the germ-band is as follows: Firstly, the tissue moves downward towards the invaginating ventral furrow (A1), then extends horizontally, before ultimately curving upwards as it encounters the back (posterior) tip of the embryo.

In general, we see great agreement between simulation and data in the final shape and placement of the germ-band. This says nothing explicit about the timing and interaction of the activities present, but it hints at the fact that the movement towards the belly, back, and top side are also recreated in our model. To get a better understanding of the agreement, we will need to look at the active aspect of the germ-band extension.

To further validate the agreement, we can focus on a neat observation: The cells in the germ-band that start further towards the back will migrate much further horizontally than the cells closer to the head, with cells next to the **cephalic furrow** only moving downwards (ventrally). This is a result of the extension being the sum of many small contributions adding to the global motion.

For a representation of the motion of individual cells in the germ-band, a random selection can be seen in Figure 3.5 below:

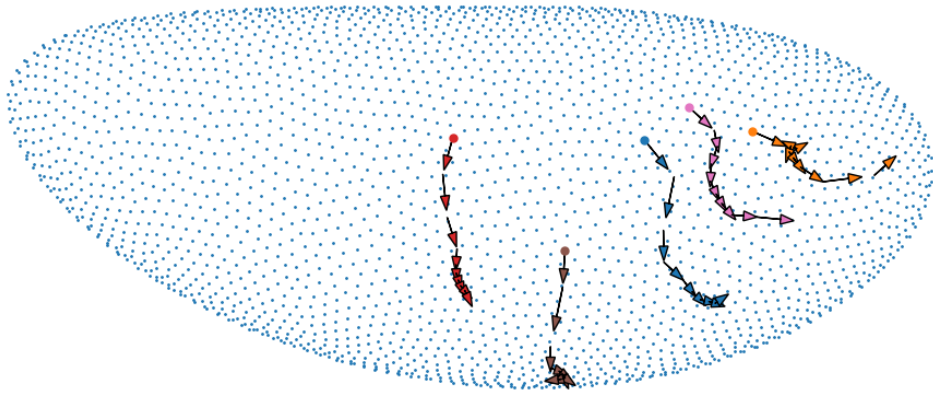


**Figure 3.5:** A number of cells from the germ-band with their migration over time visualized. The arrows correspond to movement in equally spaced time intervals during the germ-band extention (A2). It can be seen that – like in real embryos – cells that are formed closer to the posterior tip migrate more in the horizontal than vertical direction.

It can be seen that we have captured the uneven cell migration, where cells that starts further along the horizontal axis along also moves more horizontally.

For completeness sake, we have also made a stream-plot with a flow field visualizing the individual motion of all cells at once. This can be seen in Figure A.1 in the appendix.

To summarize: We have a great visual agreement in the change of tissue-scale morphology of the germ-band. The migration downwards towards the belly (ventral side) due to the furrow formation (A1), the germ-band actuating horizontal motion, and finally the ‘rise’ at the back (posterior tip) due to the boundary condition, all seems to have been captured by the model. In the single-cell case we also see a general correspondence between simulation and reality, preliminarily supporting that the tissue behaves as expected.

An examination of the dynamical timeline will have to wait till later sections, but in general, we find that our simulation has comparable morphological

changes of the second main event, the germ-band extension (**A2**).

### 3.2.3 (**A3**) The Posterior Midgut Invagination

Now, our final point of focus is also the hardest to visualize neatly. Looking at electron microscopy as below in Figure 3.6, we can get a rough idea of the motion: The back tip moves slightly upwards. Once it reaches a certain point, the tip folds in on itself as the ventral furrow reaches it, connecting the tube with the invaginating cavity.<sup>[7]</sup>

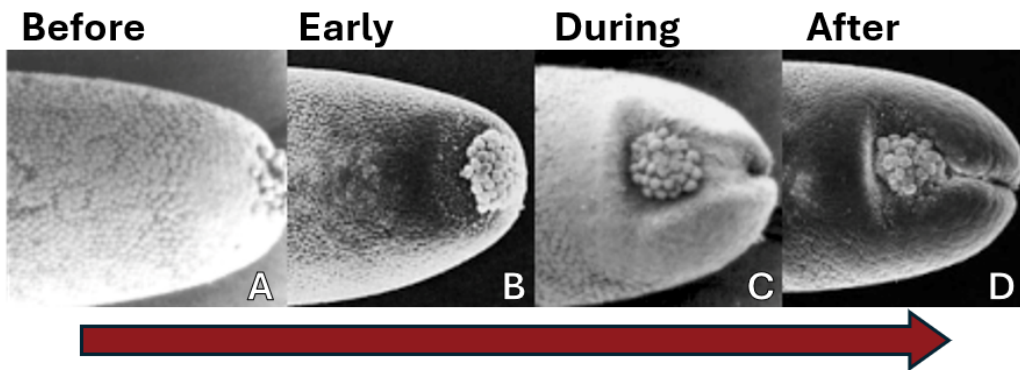


**Figure 3.6:** An overview of the *posterior midgut invagination* (**A3**) as viewed from the top (dorsal) side.

The pole cells – which are clearly visible at the posterior tip (**A**) – are moved to the top and towards the front of the embryo (**B**). As the tissue beneath them apically constrict, the newly formed indent merge with the **ventral furrow** as this reaches the posterior tip (**C**). Finally the pole cells are internalized as the furrow closes off (**D**). The time points are not linearly spaced.

(Sources: **A & C**: Sweeton et al. (1991), **B & D**: Gibert (1994))

Zooming in on the very back of our simulated embryo, we can see much of the same dynamics represented:

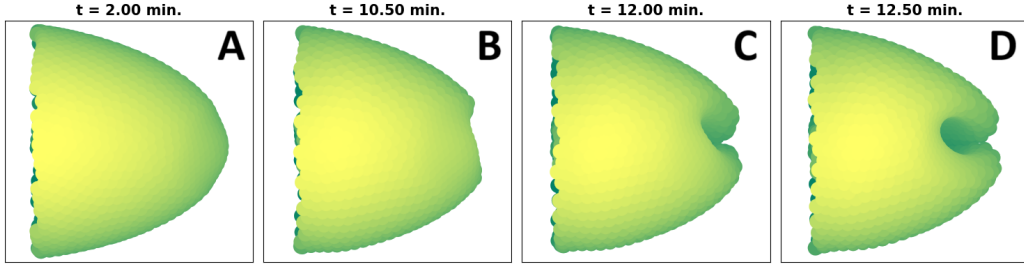


**Figure 3.7:** A zoom-in on the the top side of the posterior tip of the embryo. To to be compared with Figure 3.6.

The PMG-event (A3) goes as follows: The cells in the tip starts tightening (A), the tip then is pushed upwards (B), it then invaginates meeting the ventral furrow comes from below (C) before being moved further up (D).

The formation of the posterior midgut (A3) is an intensely studied phenomenon in *Drosophila* gastrulation, but has, to the best of our knowledge, not previously been simulated.

Visually grasping what happens *in vivo* can be tricky, as there is a distinct lack of good imaging of this phenomenon. This is caused by two things: The action happens very quickly and much of the interesting cellular dynamics happens inside, or on the border of an invagination. This point will return shortly, but visually we seem to be agreeing with the external imaging for the most part. In general we capture the motion upwards followed by both a folding and a fusion. Unfortunately, in our simulation the upwards momentum is slowed to a halt – *in vivo*, the posterior is moved much further after invagination. Through personal dialogue with Nobel laureate Erik Wieschaus, we have found that the inherent isotropy of our cell size might be to blame, as mutants with less cell-deformation experiences the same trouble.

Our frustration with a lack of good reference images hail from to the fact, that once invaginated, cells are impossible capture by ordinary microscopy. The only usable visualization of internalized cells, is of a meticulously *hand-tracked* vertical band around the posterior tip. The approximate extend of this band can be seen here:

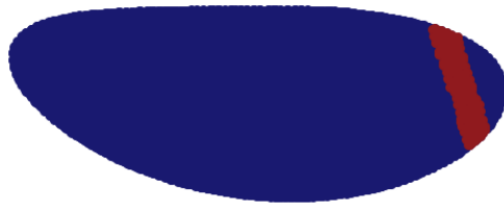


**Figure 3.8:** The approximate band as used in the following section for analyzing the deformations around the posterior midut.

As looking 'inside' our virtual embryo is trivial compared to real life, we have extracted the band of cells, trying to recreating the framing of the data. In Figure 3.9 the collected data can be seen and in Figure 3.10 the corresponding cells can be seen in simulation.

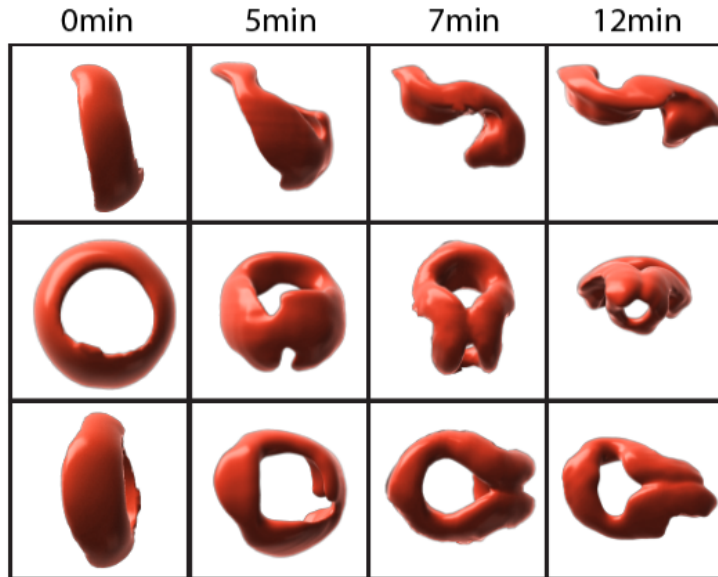


**Figure 3.9:** A 3D mesh of cells from in vivo imaging. Each row is a constant angle. (Source: Daniel Alber. Not yet published. Reproduced with permission)

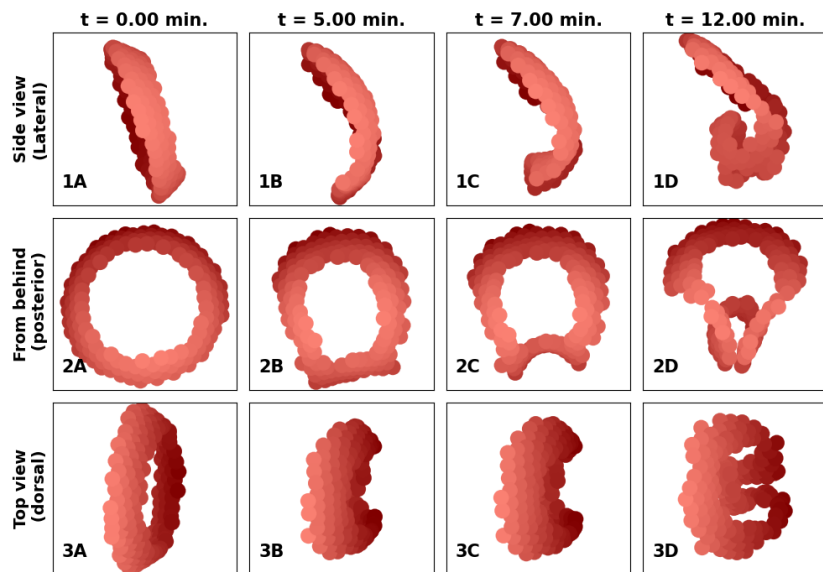


**Figure 3.10:** The approximate band of cells as displayed in Figure 3.9 extracted from our model and visualized in a comparable manner.

The combined invagination of the PMG and the ventral furrow (**A3**), is now very visible in **2C-2D**.

For the first 5-6 minutes of the timeline, simulation and reality are relatively well aligned. We see a push from the extending germ-band moving the cells towards the posterior tip. The trouble begins in **1C** and **1D** where the orientation of the cell-band should be almost horizontal. As Figure **3.10** shows, our model has not moved the cells far enough towards the top. In spite of this, as the posterior closes off, a seemingly right morphology emerge. It should also be noted that the closing happens with reasonably internal timing. In general we have a respectable qualitative agreement, albeit lack of upwards (dorsal) motion is visually evident.

Our model clearly has some fundamental flaw or inconsistency, but barring the lack of movement towards the back, we got quite close in both timing and shape. With a few exceptions, our model provides a phenomenologically faithful recreation of this vital morphogenetic event. As the posterior invagination (**A3**) requires both successful modeling of (**A1**) and (**A2**), we are, to the best of our knowledge, the first group to attempt this in silico experiment. So while our simulation is not perfect, the simple fact, that this is a world-first attempt at recreating something well-studied seems noteworthy.

### 3.2.4 General morphology

In the literature, a way of visualizing changes in both local and global structure, consist of drawing virtual lines on an embryo at the onset of gastrulation. How these lines translate and skew over time is very descriptive for the general changes in form. An example in both data and simulation can be seen in Figure **3.11**.

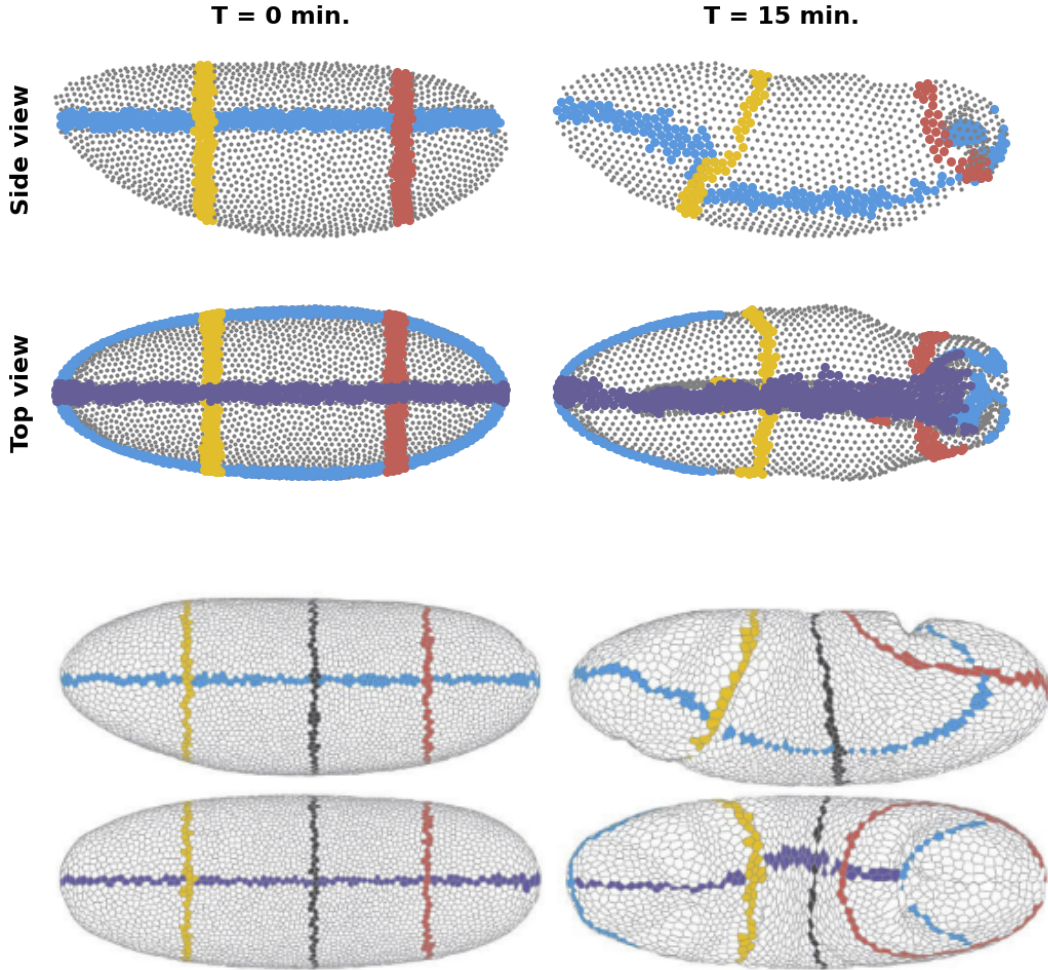


**Figure 3.11:** Positions of specific colored-in bands at two different time points.

As can be seen, the general movements align quite well, albeit with some discrepancies around the posterior tip.

**Top row:** Simulation.

**Bottom row:** Segmented images (Source: Stern et al. (2022)).

This juxtaposition allows for some interesting observations:

As is evident, there is a general agreement between both local and large-scale changes in embryonic form.

Going through the lines, color by color we might be able to surmise something about the differences in dynamics between our model and nature:

**Blue** The biggest problem plaguing our simulation is evident. The pressure from the bottom (ventral) side of the model cannot push the posterior tip. The blue line acts as a stand-in for the germ-band. Much of the analysis from its section applies with two exceptions:

- In simulation, close to the (deliberately) missing cephalic furrow (the **yellow** line), the blue line breaks up. This might be caused by lack of pressure relief in our simulation as the furrow in real life internalizes some cells.
- The second image is at a later time point than what we previously compared the germ-band to. Here the lack of upwards motion is again evident.

**Red** The same effect (lacking upwards motion) can also be seen in the red line, where it almost, but not completely reaches the rightmost (posterior) tip. It is also clear, that after invagination, the lines close to the end (red and blue) becomes muddled.

**Yellow** A helpful line for understanding the motion around the area of the cephalic furrow. The top part moves towards the back and the bottom towards the front without too much internal bending. In general great agreement.

**Purple** The mid-line seems as stable as in vivo. The "bunching up" of the **purple** in the posterior-end is most likely an artifact from the fact, that – unlike in real life – the cells are not being hidden below other tissue in the posterior invagination.

A final observation: The point cloud of our 'cells' become spread out over time. This mirrors the quite radical surface area increase each cell has in vivo, after room has been made on the surface by the various internalized tissue.

Quickly summarizing all the qualitative comparisons we have seen in this section: We have found some great agreement! From the full embryo comparison in Figure 3.1 and the individual events, the gastrulation seems to qualitatively have been recuperated well, both in timing, in the intermediate morphologies, and in the resulting structural shapes.

### 3.2.5 Timing

One of the key question we propose is whether precise timing mechanisms are necessary to drive the complex morphogenetic processes we see, or if they can emerge purely from initial conditions and cell interactions.

Cells have been shown to have remarkably precise internal clocks and chemical gradients in the embryo changing across timescales from seconds to hours[27]. There is also the "biological clock" [24] that proteins themselves have dynamic structure that can change over time.[25]. But there is no evidence for any specific timing in stages 5-7. We would like to stress the importance of the result that we seem to have recapitulated some of the long-term dynamics completely without any explicit time-dependent parameters. This could be seen to corroborate our thesis that initial conditions and an inter-cellular rule set is sufficient for exhibiting accurate emergent behavior.

### 3.3 Quantitative Agreement

While visual inspection of our simulation is interesting – and a clear result in itself, given that morphology is the target – we would like some quantification of the model performance. Having a numerical framework will allow for optimizing model parameters and in other ways objectively defining the accuracy of our solution. It also allows for statistical checks on the consistency between different runs of the simulation, helping quantify the degree of stability. Additionally, this framework would provide a foundation for testing various hypotheses regarding cellular behavior and tissue mechanics, ultimately leading to more a robust inspection of the model and maybe into insights to the underlying biological processes.

We set out with a handful of core areas we would like to explore. We wanted to determine a minimal set of rules necessary for capturing the overall gastrulation. Next, we wanted to explore whether the boundary and initial conditions alone are sufficient to drive these processes. Finally, with a (hopefully somewhat validated) model in hand, we wanted to understand what insights could be drawn about the interaction between domains.

We have already begun to address the validity of the model. We have seen how the boundary condition impact the overall shape (the posterior tip diverting the extending germ-band), and we have visually confirmed that the process unfolds in a manner consistent with what is observed *in vivo*. However, we have yet to rigorously quantify how these conditions affect key aspects such as tissue displacement, velocity, or strain involved. And, while we have found evidence for the interplay between the different parts of the embryo, we have yet to uncover the nature of the spatial domain interactions in an any way systematic or measurable way.

We will now take a step back from the individual morphological events and focus on large-scale analytics again. We can then return to the individual event, perturbing them to see how this affects the process.

### 3.3.1 Movement

Although the final result of a successfully simulated morphogenesis is a three-dimensional structure, our primary focus lies in understanding the kinetics of the system. We will therefore be going away from still-image comparisons, trying to capture the *dynamics* of the system instead. We will get to strain analyses later, but much of the biomechanics of the system can simply be captured surveying its granular cellular motions.

It has been stated multiple times that usable quantitative data is tough to come by. But very recent technical advancements in both microscopy and cell-segmentation has given rise to the possibility of large-scale, automated analyses.[29] We will take our onset in data collected in Stern et al. (2022). This dataset includes machine-tracked 3D positions of every visible cell’s center, recorded across approximately 30 time steps during gastrulation.

Since there is no standard method for labeling individual cells, we cannot make direct one-to-one comparisons between cells. To address this, we developed the following measure:

We start out by finding the displacement vector  $\mathbf{v}_n(t)$  of the in-data cell positions:

$$\mathbf{v}_n(t = \tau) = \mathbf{p}_n(t = \tau) - \mathbf{p}_n(t = \tau - 1) \quad (3.1)$$

Take each simulated cell and find the average displacement vector of the  $N$  spatially closest cells in data:

$$\boldsymbol{\mu}_i(t = \tau) = \frac{1}{N} \sum_{n=1}^N \mathbf{v}_n(t = \tau) \quad (3.2)$$

Where the sum over  $n$  is for the  $N$  nearest in-data neighbors of the simulated particle  $i$  at time step  $\tau$ .

Now in the same way as Equation 3.1 we calculate  $\mathbf{V}_i(t)$ , the recent displacement of particle  $i$ . Now using the  $\mu_i(t)$ , we introduce  $\alpha_i(t)$ :

$$\alpha_i(t = \tau) = \arccos(\mathbf{V}_i(t = \tau) \cdot \boldsymbol{\mu}_i(t = \tau)) \quad (3.3)$$

We now have an angle between cell  $i$ ’s motion and the in-vivo ”average motion vector” at this position. The resulting (acute) angle difference is between 0 and  $\pi$ .

Below (in Figure 3.12), the resulting analysis can be seen at time point just before the posterior invagination.

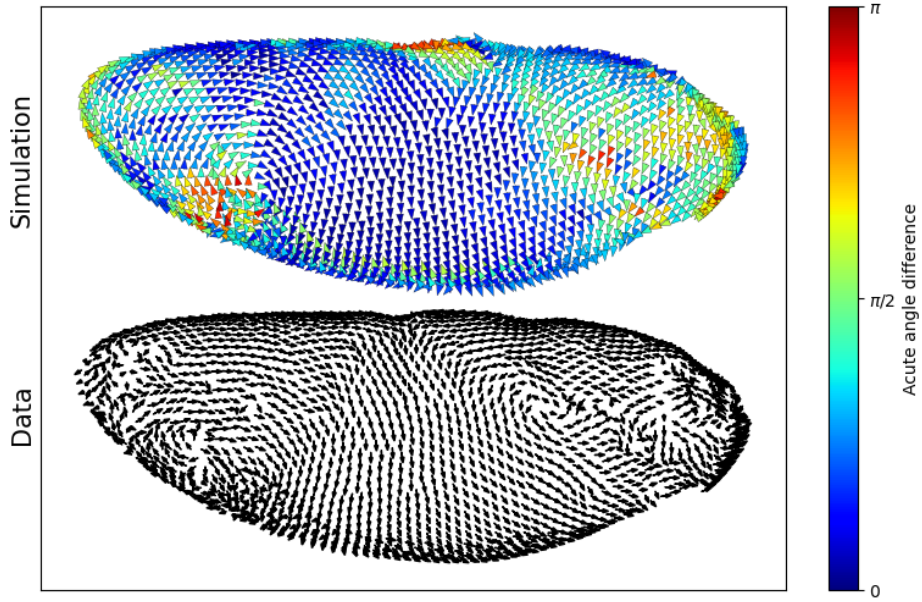


**Figure 3.12:** Snapshot of motion vectors for each cell in simulation and corresponding  $\mu_i$ . In the simulation each cell is colored according to the angular agreement  $\alpha_i$ .

It can be seen that at this specific time point, the agreement ranges from surprisingly good to predictably bad. Visualizing the  $\alpha$  metric in this way helps highlight the spatial distribution of the discrepancies. Overall, while large regions display near-perfect alignment, others suggest opportunities for refining the model, particularly it seems like the discrepancies are found in more dynamic regions.

### 3.3.1.1 Movement across time

Now, for ease of parsing, do the following transformation, introducing the metric  $\xi_i(t)$ :

$$\xi_i(t = \tau) = 1 - \alpha_i(t = \tau)/\pi \quad (3.4)$$

This allows us to score the particles on a scale of 0 to 1, where 0 is no overlap and 1 being perfect alignment with data.

Averaging this score over the whole embryo for every time point we get the following relation:

$$\delta(t) = \frac{1}{N_{cells}} \sum_{i=1}^{N_{cells}} \xi_i(t) \quad (3.5)$$

This number quantifies the average agreement for the embryo at a specific time point. Plotting this we get an estimate of the agreement to the general kinematics of the embryo. In Figure 3.13, the  $\Lambda$ -measure can be seen for every time point in the data:

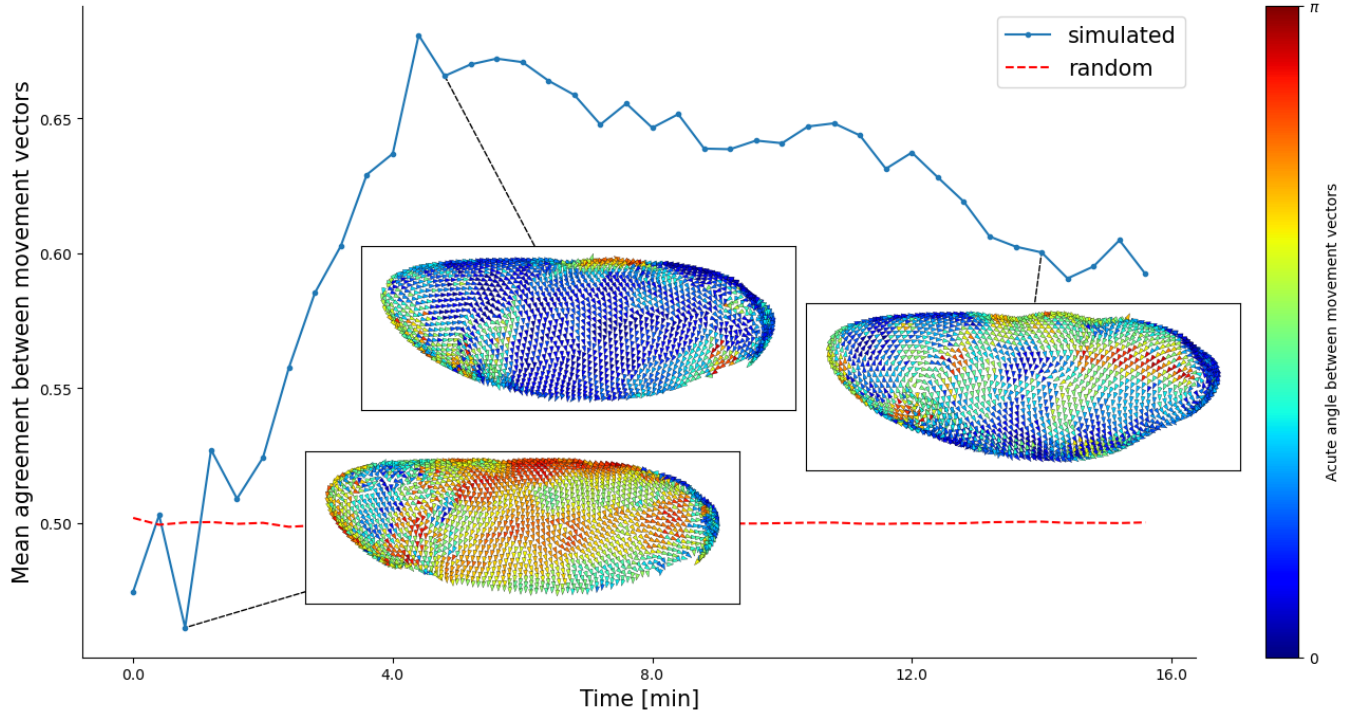


**Figure 3.13:** The average motion-vector agreement across the full embryo  $\delta(t)$  as a function of time. On the inset axes three snapshots of the spatial distribution of error along with the in-simulation motion can be seen. The red *random*-line corresponds to a simulated embryo where every direction of motion is uniformly randomly chosen.

In general, we see a consistent, well-above random overlap between data and simulation.

From the previous sections, we had some intuition that our simulation visually followed the general flow of the morphogenesis. Figure 3.13 gives us some quantitative confidence that the motion of the individual cells also align with the data. Some notes on what we can derive from the above plot:

It is very clear that in the first couple of minutes our simulation and reality does not completely agree. This will be a recurring theme. We believe this could be caused by a difference in cell-firmness between real life and our simulation. Specifically, biological cells exhibit a degree of elasticity and plasticity that is not fully represented in our model. When the ventral furrow invaginates (A1), the pulling takes some time to stretch each cell, with its center consequently lacking behind. In our model, the tissue moves down immediately and rather uniformly. Taking cell shapes more or less explicitly into account might allow for more gradual stretching, allowing the cells to adjust to tensile forces.

### 3.3.1.2 Movement across space

To find the parts on the embryo that is performing the worst, we look at the integrated error over the full run, summing over every time step.

$$\Delta_i = \frac{1}{N_{timesteps}} \sum_{\tau=1}^{N_{timesteps}} \xi_i(t = \tau) \quad (3.6)$$

This results in an "average lifetime error"  $\Delta_i$ . Mapping this back onto the initial position for cell  $i$  we can see how the error is spatially distributed:

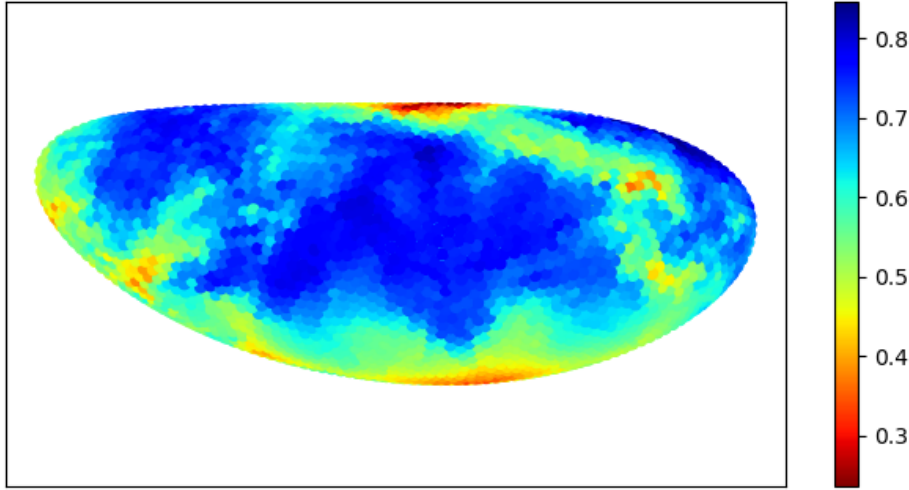


**Figure 3.14:** The motion-vector agreement across the full run  $\Delta_i$  for each cell  $i$  mapped back onto its original positions. Some domains, especially the ones on the back and belly sides of the embryo, are performing much worse than the rest.

A high  $\Delta$  indicates a strong match between simulated motions and the mean motion observed by a cell that starts at the corresponding position on the embryo surface.

Going domain by domain:

The *in silico* motion of the **germ-band** seem in great agreement with data, especially given how far the individual cell travels. We had previously found a qualitative match in overall trajectory and displacement, but this quantifiably highlights the model's ability to capture the large-scale motion of the germ-band extension (**A2**).

The **ventral furrow** and its invagination (**A1**) is a main contributor of error. Because of the way the imaging was done, all invaginations (the ventral furrow for example) will automatically have low agreement. The original data only supported motion-tracking on the exterior surface of the embryo. This limitation naturally reduces the precision of our comparisons in regions where inward movements are critical, which is one of the primary types of motion.

On top (the dorsal side), the sheet buckles and folds in vivo. This was not part of our simulation and it can also be seen that our measure of agreement is greatly penalized.

For the **posterior** part of the embryo, the agreement is surprisingly good. This is either because the cells that start at this positions makes the general motion albeit not far enough (remember displacement magnitude does not matter), or the no-inward-motion-tracking is somehow doing us a favor.

Finally, the head part of the embryo (left of the **cephalic furrow**), especially on the lower side, a lot of error accumulates. The head area was from the start deemed outside the scope of the current project, so quite a lot of disagreement is anticipated.

### 3.3.1.3 Movement across domains

Having such a large discrepancy at specific parts of the egg gives us the idea of discarding parts of the egg from the calculation.

We calculate the mean agreement-score  $\delta(t)$  just like Figure 3.13, but this time excluding cells, in the **cephalic** area, in the **ventral furrow**, or both:

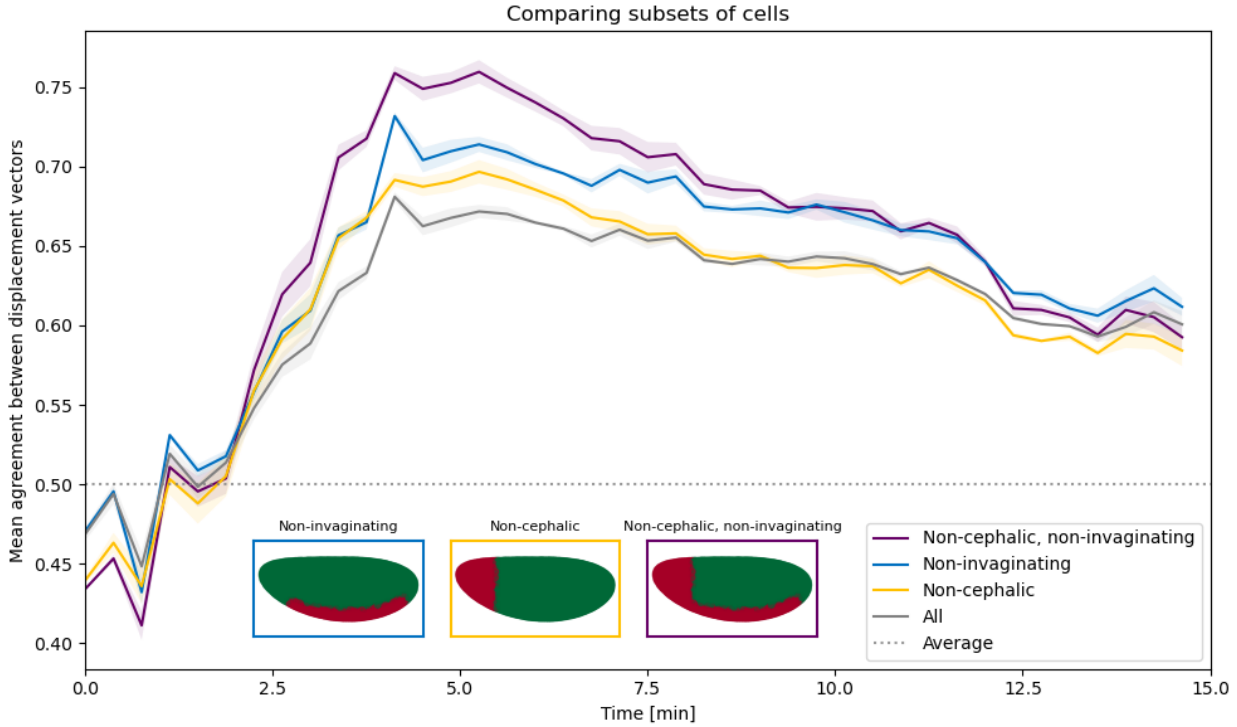


**Figure 3.15:** The motion-vector agreement across the full embryo  $\delta$  but with certain domains excluded from the calculation. For confidence in the stability of the solution, all lines and shaded areas are averages and standard deviations of three runs using identical parameters but different seeds. It is clear that excluding some domains improves the general agreement.

As can be seen in Figure 3.15, limiting the agreement analysis to only look at specific subsets of the embryo improves the performance significantly:

Once anything in the head area is discarded from the average (**Non-cephalic**), we see a noticeable bump in quality. This is true for the most of the duration, but the effect is actually reversed in the far ends of the simulation. We believe this occurs because of the relatively well-behaved cephalic region – excluding it helps boost the overall average when other regions perform well. However, when the rest of the simulation decline, removing the head slightly heightens the average quality.

Removing cells in the belly area that were apically constricting (**Non-invaginating**)

we see an even more pronounced increase. This time, the increase is, predictably, more stable, as these areas are responsible for consistently worse performance.

Combining both masks (removing both the head-region *and* the invaginating parts) gives an even better result!

To summarize: Focusing on the parts of the embryo with a good possibility of overlap with data, we get a much higher average cell-motility agreement (almost 0.8) during the dynamic phases of the simulation. The improvements are substantial and we feel it helps portray how our model can excel.

### 3.3.2 Strain

As the tissue warps and skews, the cells are both subject to- and drivers of stress and strain on the cell walls. These mechanics are some of the most widely studied parts of the in morphogenesis.

While our simulation neither includes cell walls nor explicit strain calculations, a method has been developed that only requires positions of cell-centers – and that we have! The Green-Lagrange algorithm (implemented as described in [Butler et al. \(2009\)](#)), can be applied to find local deformations in tissue. In Figure 3.16 the results of an implementation can be seen and compared to a graph on data.

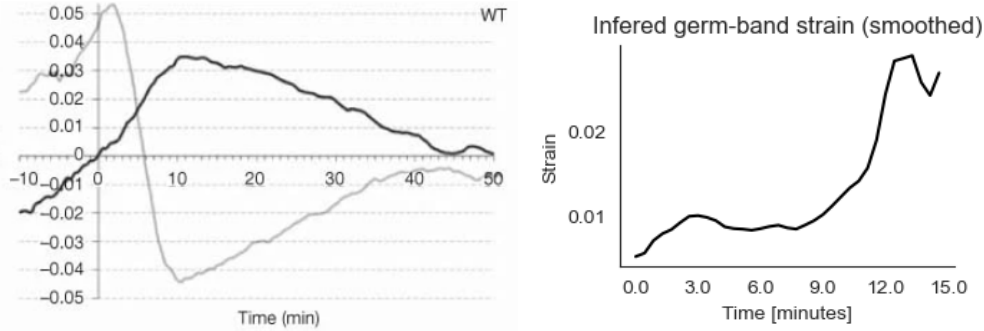


**Figure 3.16:** A comparison of estimated strain-rates as a function of time between in-vivo data and our simulation. In both cases we see a quick rise followed by a fall-off at the time of invagination of the posterior ([A3](#)) at around 12 minutes.

**Left:** A plot of the inferred strain rate (black line) in the germ-band (Source: [Butler et al. \(2009\)](#)).

**Right:** The inferred strain rate in the germ-band in simulation using the the Green-Lagrange algorithm.

In the first 12-15-minutes we observe a rising strain, ending at the point of internalization of the germ cells ([A3](#)). In our simulation, the rise in strain has a delayed onset, once again showing how the first 2 minutes have a central difference from ground truth. To remind, we previously postulated this was due to overly rigid tissue in simulation, which would also explain the too low local strain.

This section allows for a great comparison, as it highlights a fundamental discrepancy in tissue mechanics between our model and actual biological behavior. We have previously found a great visual agreement between simulation and data, but we now have some understanding of the inconsistencies relating to the fundamental mechanics.

Despite the overall success of the simulation, this divergence in strain accumulation suggests that the viscoelastic properties of the tissue are not fully captured and might require further refinement.

## 3.4 In Silico Mutants

Having a complete simulated pipeline from (simplified) morphogen to (approximate) morphogenesis, opens the door for analyses into both our model and its relation to nature.

A large branch of developmental biology consists of discovering or creating mutated embryos, examining the resulting organisms, thereby learning something about the translation from DNA, through cellular mechanics, to finished animal.[11] Our model also allows for the creation of genetically-variant embryos by changing the response to one or more of the simulated morphogens. In theory, we can make *predictions* by analyzing how variations in morphogen distribution or cell interactions affect morphogenesis in our simulation. We might be able to gain insights that could inform or direct experimental studies.

As described earlier, the questions we have posed are as follows:

We would like to see, with as few parameters as possible, how close we could get to the gastrulation seen *in vivo*. In general we have observed a good agreement, both quantitatively and qualitatively.

Secondly we wanted to see whether any explicit timing was needed for the full gastrulation. We have added no temporal dependence, with everything emerging and unfolding from the initial embryonic patterning.

Finally, given a model we are confident in, we would like to probe it about the interplay between its different spacial domains.

### 3.4.1 The mutants

As a framing device for examining the spatial interconnectedness of the gastrulation events, we introduce the 'mutants'. Each is missing a vital part of the gastrulation sequence and all have been observed in nature.

We will now explain the mutants that hinder **A1**, **A2** and **A3** respectively. Their mechanics and morphologies will be briefly explained, and the implications for our model briefly explored.

Videos of the individual runs can be found in Section **A5** in the Appendix.

### 3.4.1.1 (A1) No Ventral Furrow

When knocking out the *Twist* and *Snail* genes, which are primary organizers of apical constriction, the ventral furrow fails to form (stage **A1** on Figure 2.5).[18]

Due to the interconnectedness of the different parts of the embryogenesis, the lack of invagination on the belly (**A1**) also disrupts posterior midgut invagination (**A3**), altering the expected shape. Surprisingly, the resulting organism remains viable.[8] This comes down to the fact, that nature is resilient and the embryo still manage to invaginate the pole cells at the posterior, although the timing and morphogenetic movements are significantly disrupted. In [Zusman et al. \(1988\)](#), it is shown that, as a reaction to the missing invagination, an activation of the gene *sog* delays the process by approximately six minutes in an attempt to compensate for the disrupted gastrulation, further highlighting both the temporal sensitivity and interconnectedness of these developmental events.

We were unable to find any videos of this mutant, but our simulation can be seen in Figure 3.17 below:

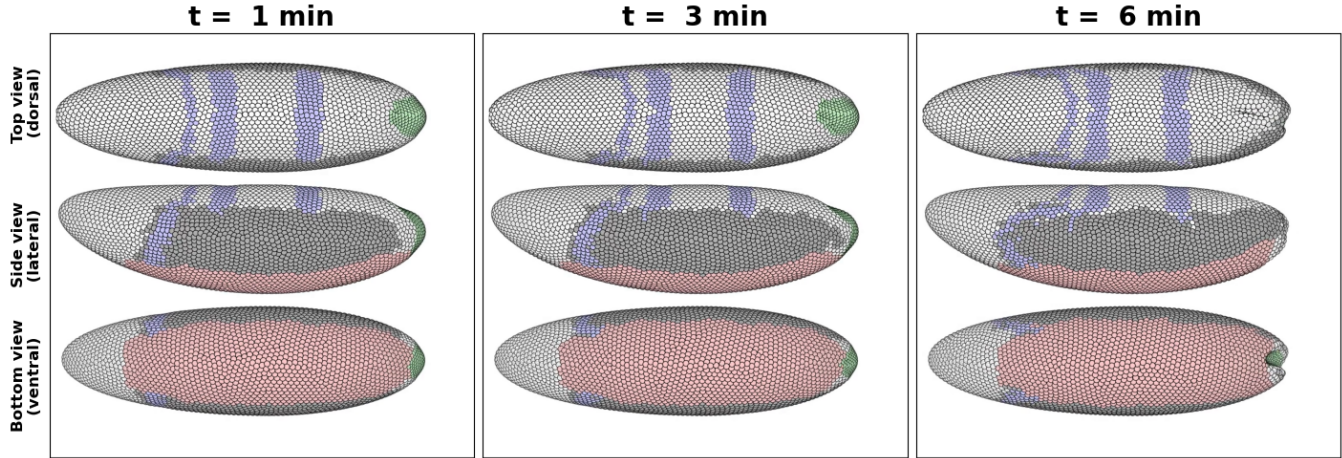


**Figure 3.17:** Three snapshots of the model simulating gastrulation, but the without the virtual gene activating ventral furrow formation (**A1**). The colors correspond to different cell types. It can be seen that the germ-band still extends horizontally (**A2**), but the posterior midgut does not invaginate correctly (**A3**) and is not moved upwards, away from the belly.

In simulation the lack of **ventral furrow** on the belly, results in the germ-band not moving downwards. As there is no compensating genetic factors in our simulation, the pressure exerted by the extending germ-band **A2** is unable to move the posterior much "upwards". This results in an invagination at the tip after about 6 minutes, after which the germ-band is moved up slightly. This can be seen in Figure 3.17.

### 3.4.1.2 (**A2**) No Germ-band

When removing the patterning that is believed to be responsible for convergent extension in the germ-band, something surprising happens. It has been shown that *Drosophila* morphogenesis is driven by more than convergent extension, and that **germ-band**-lacking-mutants are still viable: In [Butler et al. \(2009\)](#) they show that active cell elongation overtakes the responsibility for moving the tissue and the gastrulation proceeds almost uninterrupted.

In our simulation, we have no cell shape change to help alleviate the lack of motion, but as the ventral furrow without interruption invaginates (**A1**),

some movement is still seen. Figure 3.17 shows how our model fares.

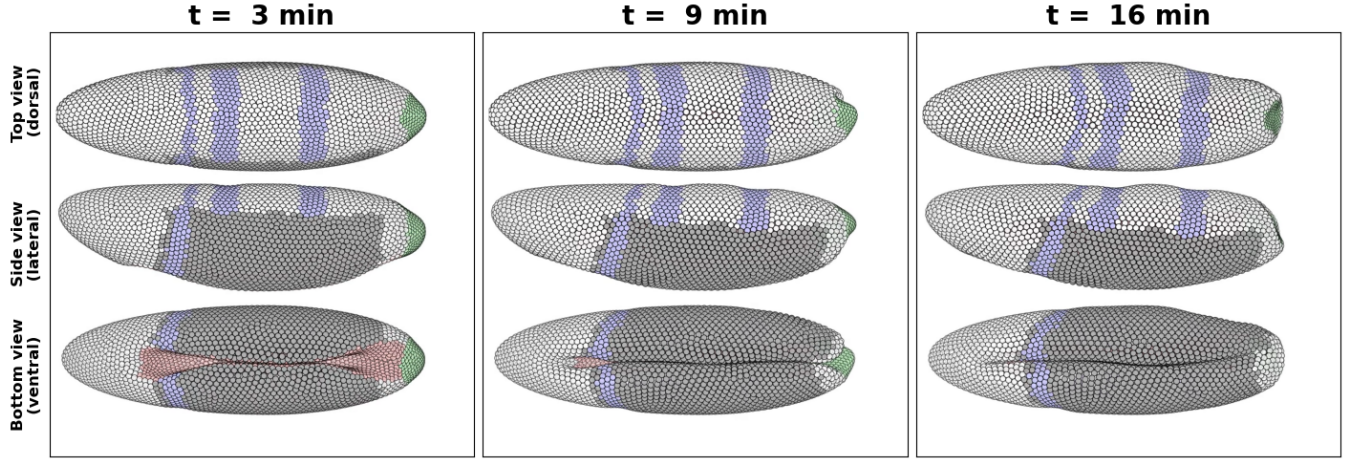


**Figure 3.18:** Three snapshots of the model simulating gastrulation, but the without the virtual gene activating germ-band exension (**A2**). The ventral furrow forms as normal (**A1**), but the posterior midgut is not internalized (**A3**) and neither it nor the germ-band are moved upwards.

Especially interesting is the following: As the posterior contracts in an attempt to internalize, it is not moved away from the narrow boundary condition on the tip, making the invagination impossible. This is a clear testament to the importance of not only having connections to the surrounding tissue, but also having an full-3D model of the boundary condition, as the resulting morphological movements are highly spatial in nature and therefore non-trivial to capture in a less general simulation. As we have no references for a "no germ-band and no ventral furrow"-double mutant, in a moment of hubris we might even propose the above behavior as a qualitative prediction for a possible biological experiment.

A final thing to note: As the posterior is not moved upwards, we observe slight twisting of the tissue during the process.

### 3.4.1.3 (**A3**) No Posterior Midgut Invagination(PMG)

The PMG is the name for the invagination that happens at the posterior to internalize the pole cells (**A3** on Figure 2.5).

In Smits et al. (2023), they show that a chemical signal from the protein *Hkb* initiates constriction on the posterior tip. In *Hkb*-deficient mutants the

lack of posterior invagination has a clear effect: The built up pressure from the extending germ-band causes the whole to twist. This has given the *Hkb*-mutant the nickname "Corkscrew".

This time we are lucky as there is a full video of the resulting mutant available. In Figure 3.19, the video of a 'corkscrew mutant' can be compared to our simulation after removing the ability for the posterior to invaginate.

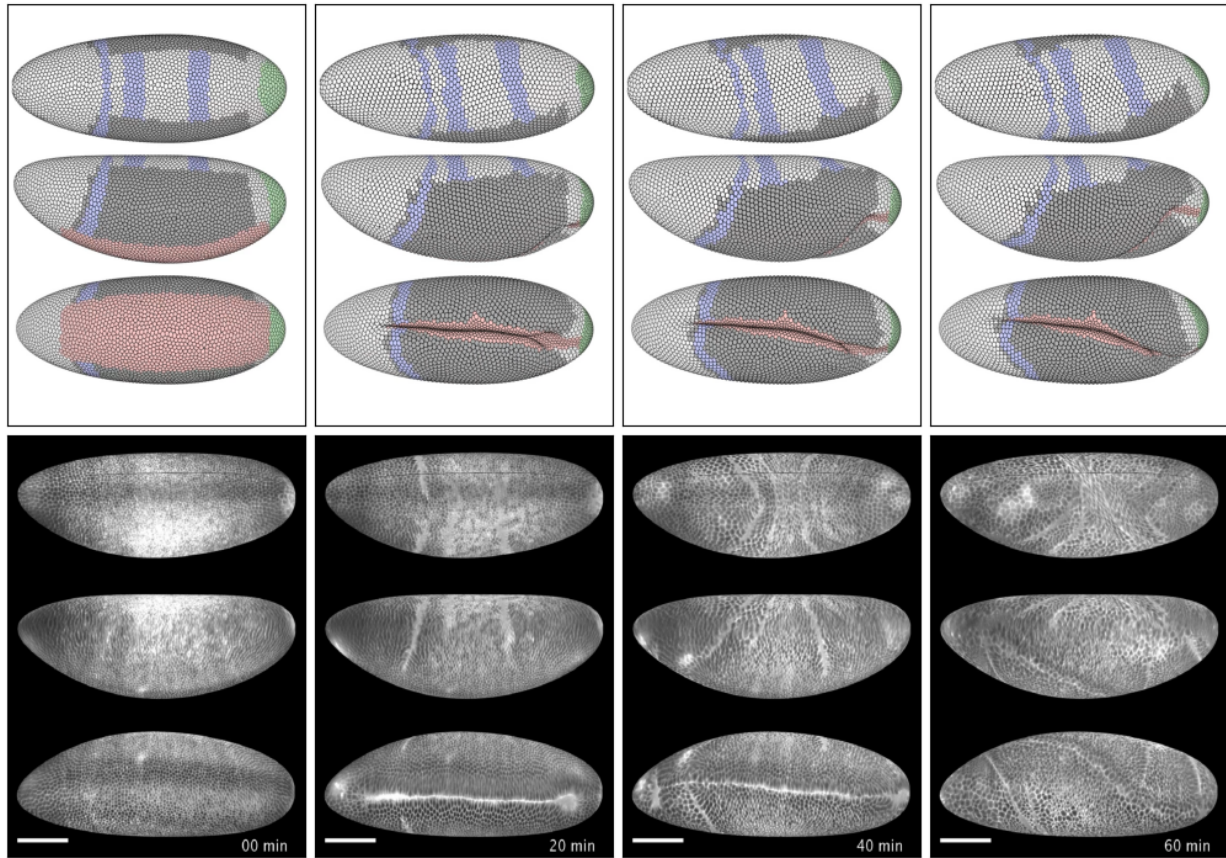


**Figure 3.19:** A purely visual comparison of the *Corkscrew* phenotype.

**Top:** Simulation colored by virtual cell type.

**Bottom:** Light sheet imaging of cell walls (Source: Smits et al. (2023))

In both cases a "twisting" motion can be seen. This is most noticeable when paying attention to the line formed by the ventral furrow.

The in vivo and in silico mutant visually agree on the motion, albeit on

different time scales. Comparing the lines formed by the ventral furrow on the belly of the embryo, we can observe the twisting phenomenon present in vivo and is also present in our in silico models. As we did not design the model with this specific simulation in mind, recuperating what is seen in vivo suggests that some fundamental tissue dynamics are captured by the model.

In general, comparing the reaction of these in silico mutants to real life phenotypes gives us a hint that our model has a somewhat correct recreation of the principles governing the cellular behavior, and is not 'overfittet' to the gastrulation it was designed to recreate.

### 3.4.2 Combining and Comparing to Benchmark

Given that we have the world's first full embryo model, we can conduct some interesting in-silico experiments. A particularly fascinating aspect of morphogenesis across all species is the interplay between the various spatially separated regions of the embryo. To our knowledge, the ability so observe the reaction in passive regions by their dynamic neighbors has not been a focus of any previous in silico experiments.

In this section, we will analyze how these regions interact and influence each other and the final outcome. We will be doing this analysis in two parts: Firstly by comparing the different virtual 'phenotypes' to our in silico baseline. Secondly by comparing to the in vivo motion data.

#### 3.4.2.1 Pole Cell Migration

We will start out by introducing the metric *Pole Cell Migration* as a virtual quantification for the success of the gastrulation. The Pole Cell Migration (PCM) is defined as the angle change of the posterior tip in the lateral plane. That is, in degrees, how far around the embryo the posterior has moved. In Figure 3.20 this is sketched out.

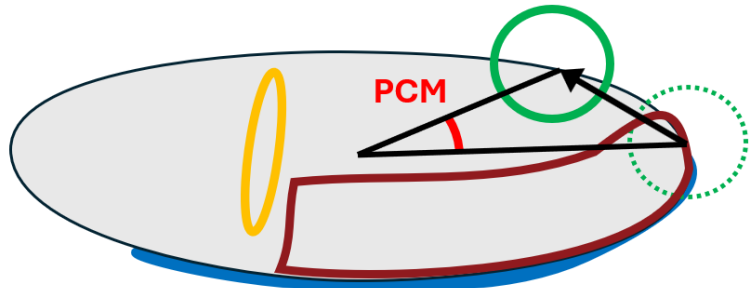


**Figure 3.20:** A diagram of the calculation of the PCM-metric. The primary domains are drawn in in.

PCM is calculated as the angle between center of embryo and initial and final position of the posterior tip respectively.

Using the above metric, we can condense one of the main motions of the gastrulation (the translation of the posterior tip to the back-side) down to a single number. In Figure 3.21 a comparison of multiple runs of the known mutants described earlier can be seen and compared to the wild-type.

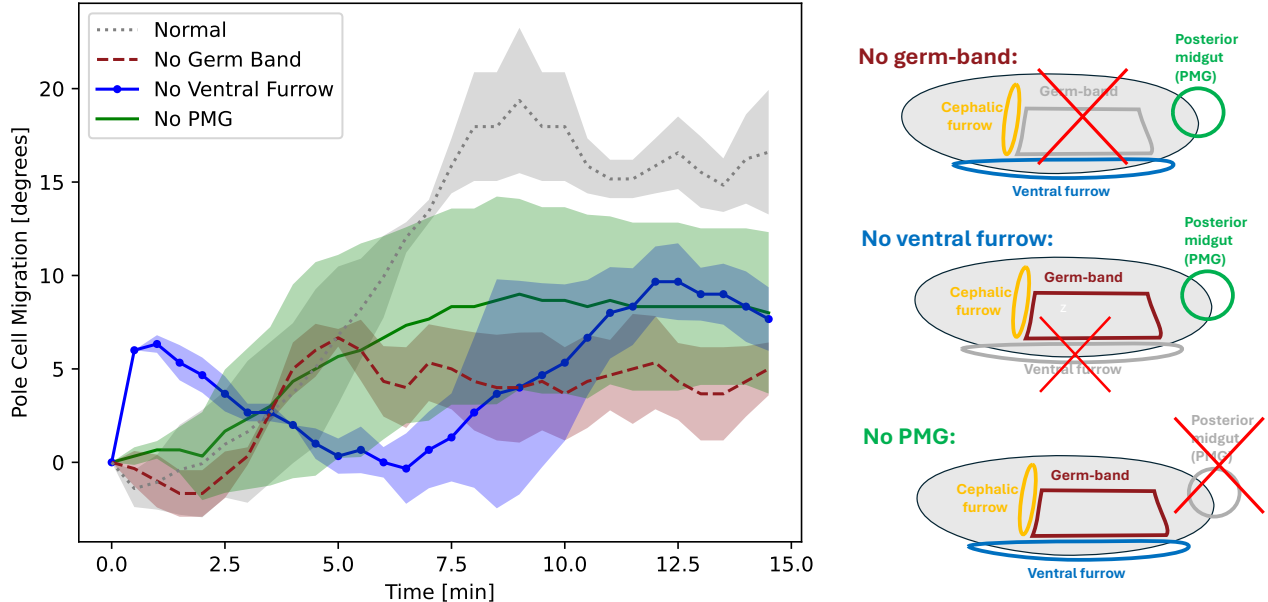


**Figure 3.21**

The mutants have been individually explained earlier, but a lot of the dynamics of the system can be gathered from the motion of the posterior tip. At risk of repeating ourselves, we can see that:

**Normal (grey):** This is the normal run. A ramping movement until reaching the point of posterior invagination just below 20 degrees.

**No germ-band (red):** At first the tip moves downwards towards the invaginating ventral furrow. When the belly convergently extends, there is a tendency to move the tip dorsally, but there is not enough force for the posterior tip to progress more than 5 degrees.

**No ventral furrow (blue):** Firstly, when no tissue is pulled into the bottom side, the germ-band pushes the posterior tip 'from the sides' instead of from the bottom. This results in a slight upwards motion in the PCM followed by a dip. In real life, after a delay, the system is overdetermined and other actions overtake to eventually shift the

posterior upwards, allowing the process to proceed. Interestingly, even with this altered timing and mechanical dynamics, the posterior region still manages to achieve its upward shift, and the embryo remains viable.

**No PMG (green):** Here we see a possible breakdown of this metric. None of the corkscrew-twisting is captured and the lowering of PCM does not capture just how unviable an embryo with this mutation is.

This section was mainly included to show the potential of having a quantifiable metric ala PCM. Because of the generality of the pipeline we have set up, in the future, a more complex simulation including more active events, folds etc. can have easily have their 'mutants' added to this graph simply by defining which gene-responses to disregard. Having a numerical criterion would also allow for intersections (both removing **A1** and **A2**, for example) to be measured against a benchmark.

### 3.4.3 Combining and comparing to Data

While comparing models internally is interesting and can say a lot about the dynamics, we wanted a short detour, recreating Figure 3.13, seeing how each mutation changes the motion-vectors. The results can be seen in Figure 3.22 below:

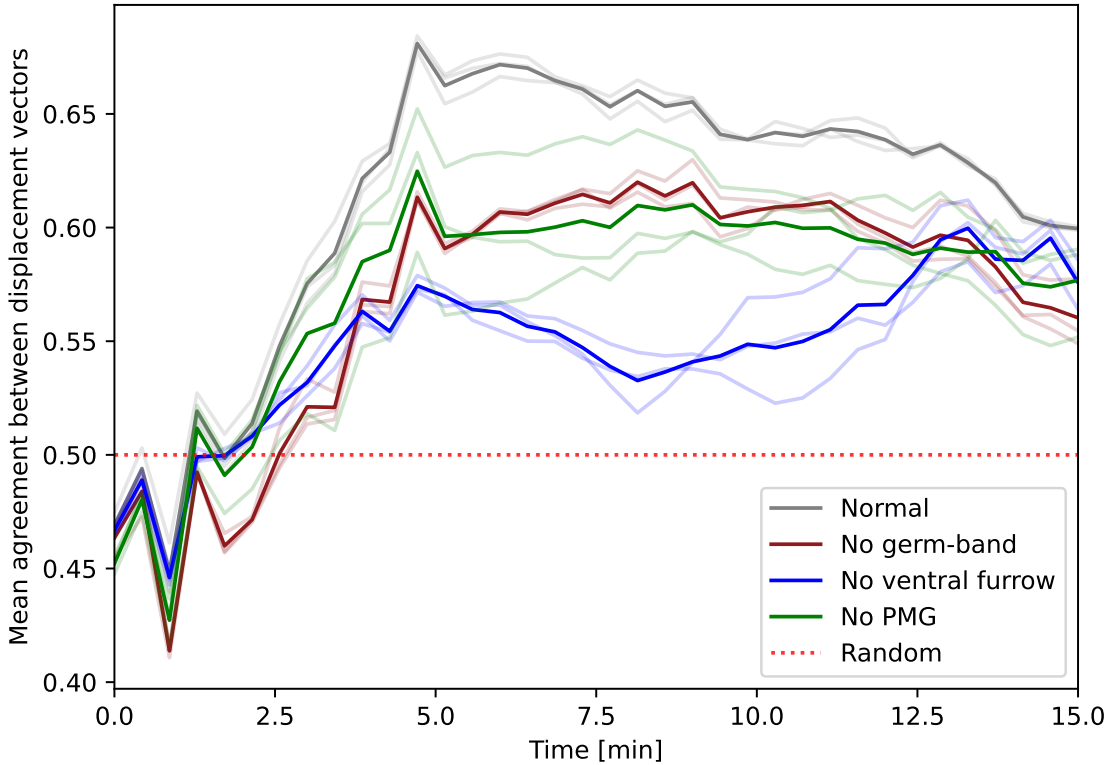


**Figure 3.22:** A comparison of the motion vector overlap  $\Delta$  for the different established mutants. Y-axis defined like Figure 3.13.

It is comforting to see that the motion agreements are all above-random but below the normal benchmark.

The "No Germ-band" and "No PMG"-mutants (**A2** and **A3**) performs surprisingly well. We think this is due to the fact that only the angles between the motions matter: If the cell-sheet moves along the right direction, it does not matter whether the sheet moves far enough or fast enough.

Removing the ventral furrow (**A1**) is by far the most disruptive perturbation to the embryo when looking at these displacement vectors. This is explained by the fact that the downwards movement (towards the ventral furrow) is

characteristic. The fact that the mutant lacking a ventral furrow invagination is performing better than the germ-band-less mutant corroborates the previously proposed idea that our germ band is pulled downwards too far too quickly.

In Figure 3.23 below, we have quantified the motion-vector agreement for the best run of our model at three different time points and mapped it back onto the original embryo. This is then also done for the different, above mentioned, mutants, and the difference is visualized.

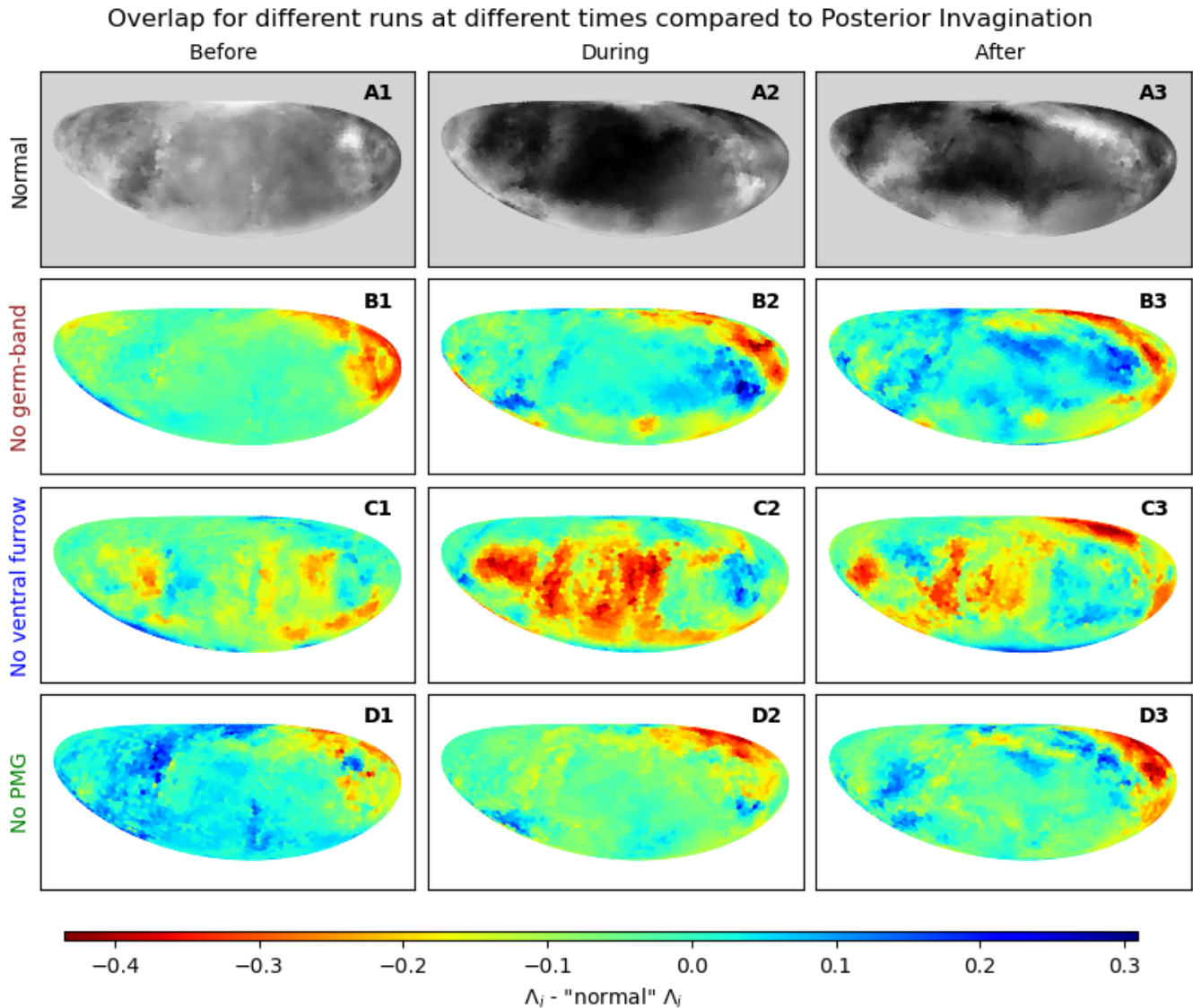


**Figure 3.23:** The difference in the  $\Delta$  measure (as defined in Equation 3.6) for three virtual mutants and the unperturbed gastrulation. Top row has different color scale where white is high disagreement. It can be seen that disrupting a morphogenetic event has cascading errors that greatly affect the accuracy of other, separate events.

We can use Figure 3.23 to do the combined analysis: When, where, and how much are each mutation disruptive for the normal flow of gastrulation. We inspect it row by row:

**Normal:** The *normal* run has already been discussed. We are here using it as a be a benchmark/reference.

**No germ-band:** The absence of an active germ-band proved to be less problematic than initially expected. The current analysis reveals that a large part of the germ-band's agreement with reality was due to its downward motion. It is very clear though, that the posterior tip – which had a great agreement in the *normal* run – is acting much worse when comparing to data. In previous sections, it was clear that this mutation disrupted the posterior midgut (PMG), leading to observable changes. Curiously, the small diagonal band between germ-band and posterior that originally had now agreement (as can be seen in A3) has improved. This might be some complex interaction between the posterior and the lateral sides of the embryo, but it could also be a sign that our implementation of the active germ-band has some room for improvement.

**No ventral furrow:** As already seen in Figure 3.22, removing the ventral furrow has by far the most severe impact for the simulation's ability to reproduce "normal" gastrulation. The ventral furrow is critical in the first large-scale movement and, in our simulation, vital for directing the germ-band. Without it, our model struggles to simulate the correct spatial deformations. It has been experimentally shown that the active convergent extension in the germ-band is in neither dependent on nor affected by the pulling force from the invagination on the lower side of the embryo.[20]

**No PMG:** Removing **PMG** leads, unsurprisingly, to significant simulation errors at the posterior end – a place where our simulation so far has seemed to be quite well aligned with data. Surprising is it, that it seems as if the performance in the head area (left of the **cephalic** furrow) is quite significantly improved. It seems the lack of relief of pressure towards the back side will improve the front.

The fact that loosing **A1** gave a much higher error in the germ-band, loosing **A2** a lot higher error in the PMG, and loosing **A3** improved the front part of the embryo, helps elucidate the complex complementary and interdependent domain- and event interactions!

# Chapter 4

## Conclusion

Even though it is often hard to grasp, the interactions between individual elements and their collective emergent behavior are defining for many natural systems. In drug discovery, understanding the interplay between the microscopic and the macroscopic is vital; changes occur on minute intracellular dynamics – with large-scale effects on organ, human, or even population scale.

Through examining the physics of the cell, biology of gastrulation, and computer science of pre-existing in silico solutions, we have proposed a simple and biologically sensible computer model. Using data of the genetic expression in the fruit fly embryo, the gastrulation was condensed to depend on only a handful of parameters on single cell level.

Using a novel approach for the field, our off-grid agent-based model allows for a full-embryo simulation of the *Drosophila* morphogenesis. This leads to a range of new possible analyses which have never been performed before: An in silico recreation of the much-studied posterior midgut invagination, and an examination of the interaction between both active and reactive domains of the embryo.

The solution was validated by large-scale visual analyses of the temporally evolving morphology. By identifying a number of key dynamic events in the embryogenesis, the timeline was compared to known *in vivo* phenomena. We have found general qualitative agreement, albeit with some obvious shortcomings, mainly the absence of anisotropy in cellular shape.

After visual verification of the model, a number of numerical metrics were devised to quantify the agreement between simulation and reality. These metrics grant us quantitative evidence of our model’s ability to correctly recuperate the gastrulation. Finally, we introduced known and unknown mutants, observed the model response, and analyzed the ramifications of these perturbations.

Turing showed that simple interplay between chemicals can create arbitrarily complex biopatterning. We have taken a step toward demonstrating how minimal, axiomatic environmental information, and straightforward, naturally feasible single-cell rules can lead to the creation of physical form.

# Bibliography

- [1] Rachele Allena, A-S Mouronval, and Denis Aubry. Simulation of multiple morphogenetic movements in the drosophila embryo by a single 3d finite element model. *Journal of the mechanical behavior of biomedical materials*, 3(4):313–323, 2010.
- [2] Philip W Anderson. More is different: Broken symmetry and the nature of the hierarchical structure of science. *Science*, 177(4047):393–396, 1972.
- [3] Kathryn Atwell, Zhao Qin, David Gavaghan, Hillel Kugler, E Jane Albert Hubbard, and James M Osborne. Mechano-logical model of *C. elegans* germ line suggests feedback on the cell cycle. *Development*, 142(22):3902–3911, 2015.
- [4] Amir J Bidhendi, Bara Altartouri, Frédéric P Gosselin, and Anja Geitmann. Mechanical stress initiates and sustains the morphogenesis of wavy leaf epidermal cells. *Cell Reports*, 28(5):1237–1250, 2019.
- [5] Mary Bownes. A photographic study of development in the living embryo of *drosophila melanogaster*. *Development*, 33(3):789–801, 1975.
- [6] Lucy C Butler, Guy B Blanchard, Alexandre J Kabla, Nicola J Lawrence, David P Welchman, L Mahadevan, Richard J Adams, and Benedicte Sanson. Cell shape changes indicate a role for extrinsic tensile forces in *drosophila* germ-band extension. *Nature cell biology*, 11(7):859–864, 2009.
- [7] José A Campos-Ortega and Volker Hartenstein. *The embryonic development of Drosophila melanogaster*. Springer Science & Business Media, 2013.

- [8] Vito Conte, Florian Ulrich, Buzz Baum, Jose Munoz, Jim Veldhuis, Wayne Brodland, and Mark Miodownik. A biomechanical analysis of ventral furrow formation in the *drosophila melanogaster* embryo. *PLoS one*, 7(4):e34473, 2012.
- [9] Jamie A Davies. *Mechanisms of morphogenesis*. Elsevier, 2023.
- [10] SF Gilbert. The genetics of axis specification in *drosophila*. *Developmental Biology*, pages 531–574, 1994.
- [11] Darren Gilmour, Martina Rembold, and Maria Leptin. From morphogen to morphogenesis and back. *Nature*, 541(7637):311–320, 2017.
- [12] Ryan S Gray, Isabelle Roszko, and Lilianna Solnica-Krezel. Planar cell polarity: coordinating morphogenetic cell behaviors with embryonic polarity. *Developmental cell*, 21(1):120–133, 2011.
- [13] Ryan M Holly, Lauren M Mavor, Zhongyuan Zuo, and J Todd Blankenship. A rapid, membrane-dependent pathway directs furrow formation through rala in the early *drosophila* embryo. *Development*, 142(13):2316–2328, 2015.
- [14] Nikos Karaiskos, Philipp Wahle, Jonathan Alles, Anastasiya Boltengagen, Salah Ayoub, Claudia Kipar, Christine Kocks, Nikolaus Rajewsky, and Robert P Zinzen. The *drosophila* embryo at single-cell transcriptome resolution. *Science*, 358(6360):194–199, 2017.
- [15] Julius B Kirkegaard, Bjarke F Nielsen, Ala Trusina, and Kim Sneppen. Self-assembly, buckling and density-invariant growth of three-dimensional vascular networks. *Journal of the Royal Society Interface*, 16(159):20190517, 2019.
- [16] Deqing Kong, Fred Wolf, and Jörg Großhans. Forces directing germ-band extension in *drosophila* embryos. *Mechanisms of development*, 144:11–22, 2017.
- [17] Matej Krajnc, Sabyasachi Dasgupta, Primož Ziherl, and Jacques Prost. Fluidization of epithelial sheets by active cell rearrangements. *Physical Review E*, 98(2):022409, 2018.

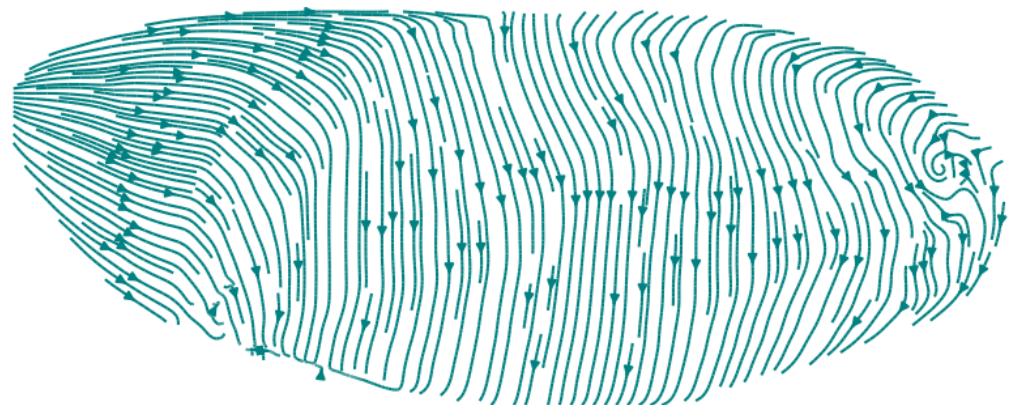
- [18] Maria Leptin. twist and snail as positive and negative regulators during drosophila mesoderm development. *Genes & development*, 5(9):1568–1576, 1991.
- [19] Dinah Loerke and J Todd Blankenship. Viscoelastic voyages—biophysical perspectives on cell intercalation during drosophila gastrulation. In *Seminars in cell & developmental biology*, volume 100, pages 212–222. Elsevier, 2020.
- [20] Claire M Lye, Guy B Blanchard, Jenny Evans, Alexander Nestor-Bergmann, and Bénédicte Sanson. Polarised cell intercalation during drosophila axis extension is robust to an orthogonal pull by the invaginating mesoderm. *PLoS Biology*, 22(4):e3002611, 2024.
- [21] Adam C Martin, Michael Gelbart, Rodrigo Fernandez-Gonzalez, Matthias Kaschube, and Eric F Wieschaus. Integration of contractile forces during tissue invagination. *Journal of Cell Biology*, 188(5):735–749, 2010.
- [22] Bjarke Frost Nielsen, Silas Boye Nissen, Kim Sneppen, Joachim Mathiesen, and Ala Trusina. Model to link cell shape and polarity with organogenesis. *IScience*, 23(2), 2020.
- [23] Silas Boye Nissen, Steven Rønhild, Ala Trusina, and Kim Sneppen. Theoretical tool bridging cell polarities with development of robust morphologies. *Elife*, 7:e38407, 2018.
- [24] Johan Olsen, Rasmus Kern, Niklas Schneidermann, Terkel Møhl, and Anders Ramhede. Lorteparforhold! *Friværdi*, 3:7–8, 2005.
- [25] Johan Olsen, Kaare Teilmann, and Birthe B Kragelund. Functional aspects of protein flexibility. *Cellular and Molecular Life Sciences*, 66:2231–2247, 2009.
- [26] Adam C Paré and Jennifer A Zallen. Cellular, molecular, and biophysical control of epithelial cell intercalation. *Current topics in developmental biology*, 136:167–193, 2020.
- [27] Stanislav Y Shvartsman, Mathieu Coppey, and Alexander M Berezhkovskii. Dynamics of maternal morphogen gradients in

- drosophila. *Current opinion in genetics & development*, 18(4):342–347, 2008.
- [28] Celia M Smits, Sayantan Dutta, Vishank Jain-Sharma, Sebastian J Streichan, and Stanislav Y Shvartsman. Maintaining symmetry during body axis elongation. *Current Biology*, 33(16):3536–3543, 2023.
  - [29] Tomer Stern, Stanislav Y Shvartsman, and Eric F Wieschaus. Deconstructing gastrulation at single-cell resolution. *Current Biology*, 32(8):1861–1868, 2022.
  - [30] Willy Supatto, Amy McMahon, Scott E Fraser, and Angelike Stathopoulos. Quantitative imaging of the collective cell movements shaping an embryo. In *2008 42nd Asilomar Conference on Signals, Systems and Computers*, pages 61–63. IEEE, 2008.
  - [31] Dari Sweeton, Suki Parks, Michael Costa, and Eric Wieschaus. Gastrulation in drosophila: the formation of the ventral furrow and posterior midgut invaginations. *Development*, 112(3):775–789, 1991.
  - [32] Alan Turing. The chemical basis of morphogenesis. *Philosophical Transactions of the Royal Society B*, 237:37–72, 1952.
  - [33] Alexey Veraksa, Miguel Del Campo, and William McGinnis. Developmental patterning genes and their conserved functions: from model organisms to humans. *Molecular genetics and metabolism*, 69(2):85–100, 2000.
  - [34] Elise Walck-Shannon and Jeff Hardin. Cell intercalation from top to bottom. *Nature reviews Molecular cell biology*, 15(1):34–48, 2014.
  - [35] Jennifer A Zallen and Eric Wieschaus. Patterned gene expression directs bipolar planar polarity in drosophila. *Developmental cell*, 6(3):343–355, 2004.
  - [36] Susan B Zusman, Dari Sweeton, and Eric F Wieschaus. short gastrulation, a mutation causing delays in stage-specific cell shape changes during gastrulation in drosophila melanogaster. *Developmental biology*, 129(2):417–427, 1988.

# Appendix A

## Appendix

### A1 Unused plots



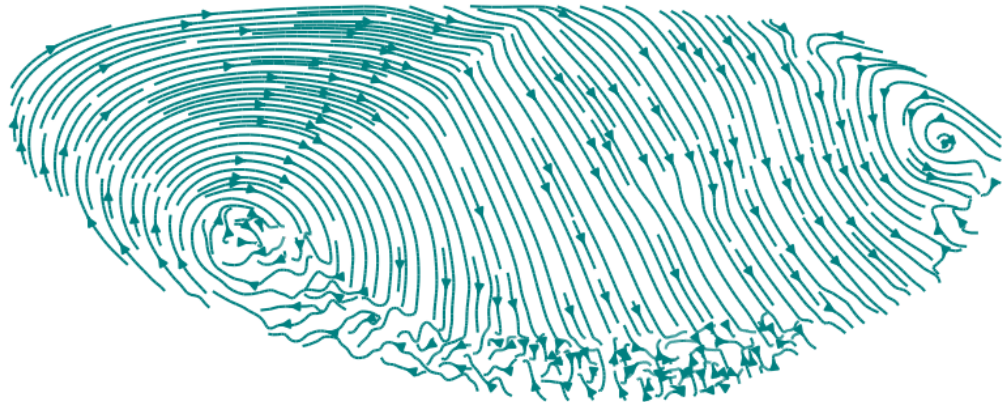


**Figure A.1:** Without any basis of comparison this flow-field is not easy to interpret, but it looks cool.

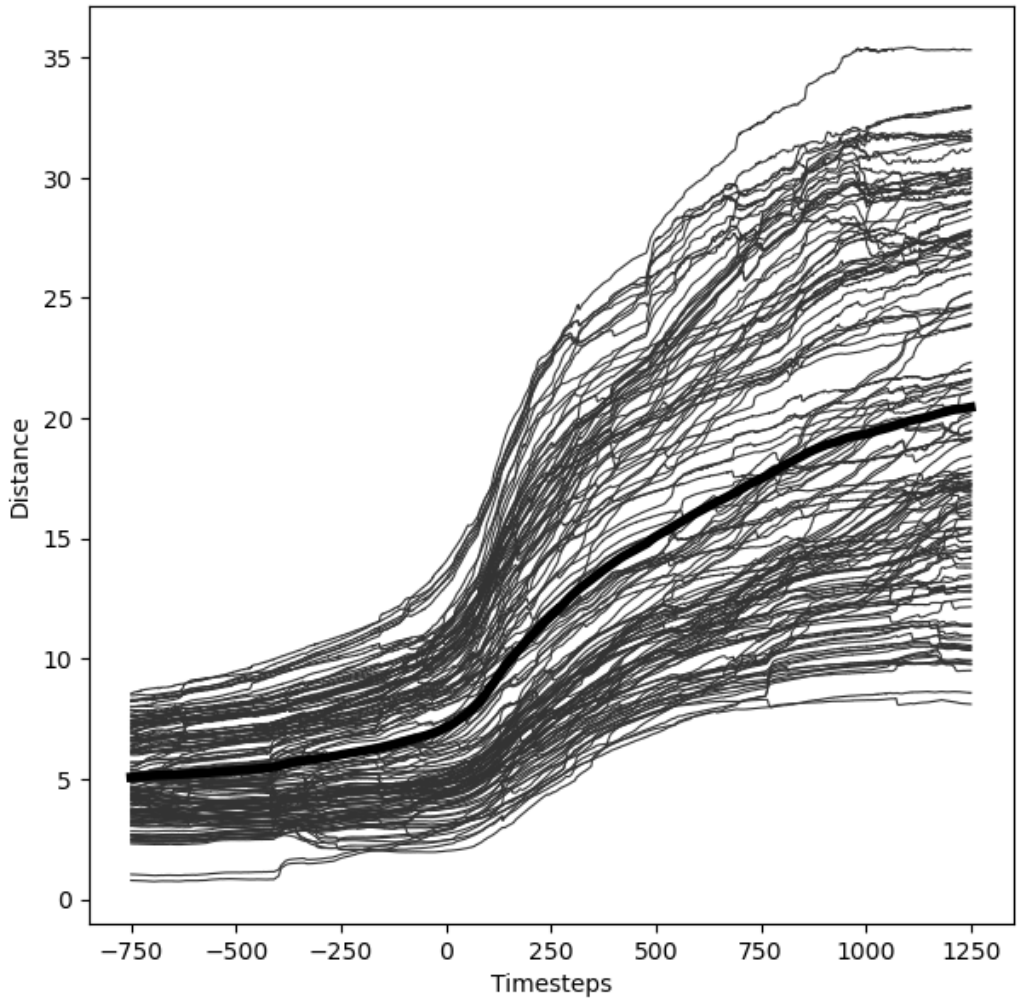


**Figure A.2:** Horizontal-position of a line of germ-band cells, mirroring the analysis in <https://www.ncbi.nlm.nih.gov/pmc/articles/PMC2801059/>

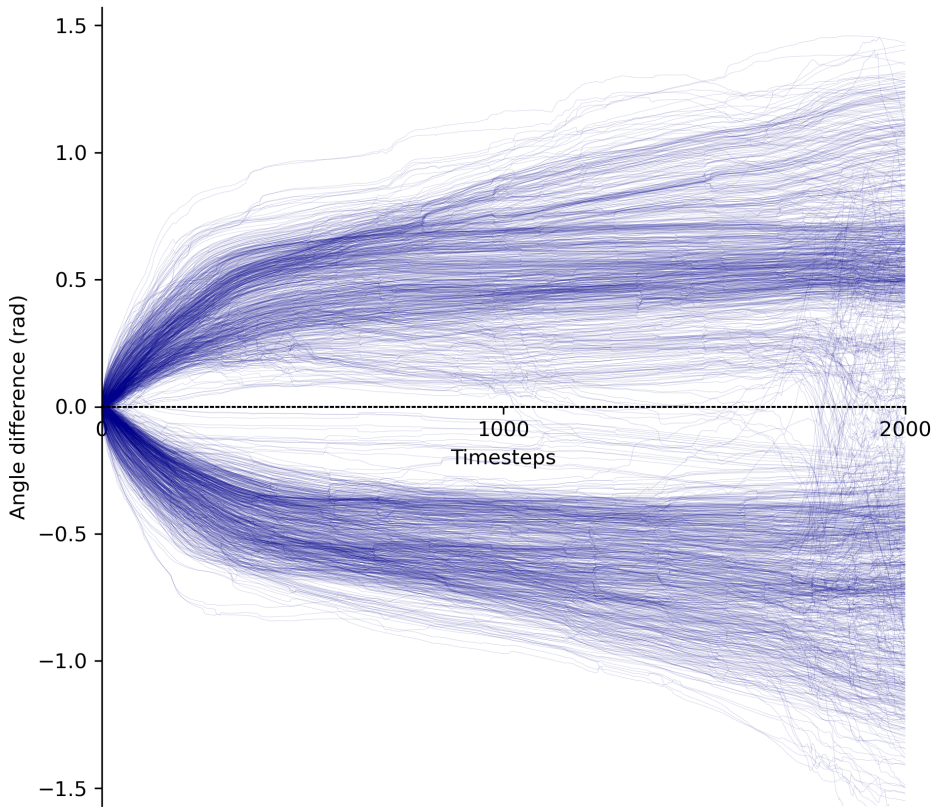


**Figure A.3:** Angle in cylindrical coordinates of germ-band. Mirroring <https://www.ncbi.nlm.nih.gov/pmc/articles/PMC2801059/>

## A2 Parameter Sensitivity Analysis

No good examination of a model is complete without a Parameter Sensitivity Analysis:

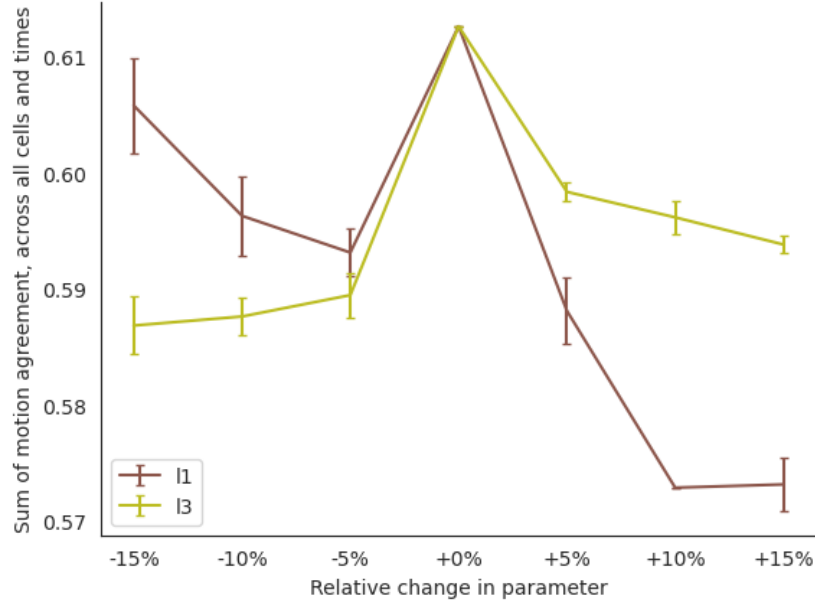


**Figure A.4:** The sum of the  $\Delta$ -metric as described in the results section. Error bars are mean and standard deviations of two runs using identical parameters but different seeds.

In general, the solution is quite stable for perturbations to the two main parameters  $\lambda_1$  and  $\lambda_3$ .

As can be seen, having a too high  $\lambda_1$  lowers the internal pressure and therefore deforms the embryo and changes the timing. Lowering  $\lambda_1$  seems to not be too bad, but the increased pressure exaggerates all invaginations quite dramatically.

Modifying  $\lambda_3$  causes more understandable changes to the morphology (the error bars are also smaller). This comes down to the fact that  $\lambda_3$  simply changes the pushing force of the germ-band during its elongation ([A2](#)). Any change messes up the timing in its interactions with [A1](#) and [A3](#). In reality, the embryo has some self-correcting effects our model does not capture.

### A3 Ventral Furrow

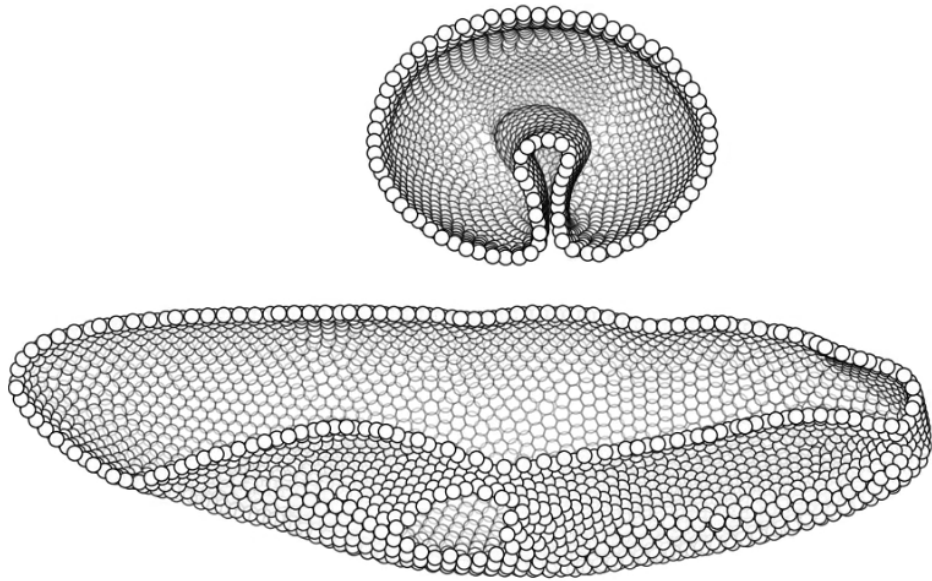


**Figure A.5:** Just before the posterior midgut invaginates ([A3](#)). As can be seen, the ventral furrow, which is supposed to go no further than halfway up extends too much into the embryo.

Note: The apparent hole in the internalized furrow is an artifact of cutting the cells in a plane.

### A4 Code details

By far the heaviest load, so optimizing this is the highest priority. Firstly, new neighbours are only found every 50th time step. Secondly, the search space is reduced by querying using SciPy's `cKDTree`. Finally, Voronoi neighbors are changed to "approximate line of sight neighbors" giving phenomenologically the same results while being magnitudes faster to calculate. The algorithm can be seen below:

```
# dx = direction vectors
# d = distances
# n_neighbors = 0 for nearest neighbors, 1 for neareast and
# second nearest, and so on
```

```
# Calculate pairwise midpoints between the cells
n_dis = torch.sum((dx[:, None, :] / 2 - dx[None, :, :]) ** 2,
                  dim=3)

# add a large constant to the diagonal for no self-
# intersections
n_dis += 1000 * torch.eye(n_dis.shape[1])[None, :, :]

# Find all cells that are closer than halfway to any other.
#   this effectively finds Voronoi neighbors.
z_mask = torch.sum(n_dis < (d[:, :, None] ** 2 / 4), dim=2) <
          n_neighbors
```

The rest of the code base can be found on: <https://github.com/JakobSchauser/Thesis/>

## A5 Videos

The videos of the different simulated mutants can be found here:

<https://github.com/JakobSchauser/Thesis/tree/main/FinalVideos/Mutants/>

## A6 Green-Lagrange strain inference

Firstly transform into cylindrical coordinates. Then implement strain rate as follows:

A strain rate is the ratio of the change in length to the original length, divided by the time interval, with units of proportion (pp) per minute.

## A7 We have not taking the following into account

### A7.1 Cell shape change

### A7.2 Pressure-buckling of dorsal folds

### A7.3 Pressure from yolk

## A8 Detailed morphogens

Genetically patterned transcription factor proteins	Location at gastrulation	Vital for development of
Twist & Snail	Ventral	Mesoderm
Huckebein & Tailless	Posterior	Endoderm (Midgut)
Runt & Even skipped	Germ Band	All of the above
Buttonhead & Even skipped	Cephalic furrow	Cephalic furrow

**Table A.1:** The most important morphogens and their simplified reason of significance

```
# The germ band requires striping to be active [citation]
GB = GE.or_gene(GE.gene("eve"), GE.gene("run"))

# A cutoff was needed because of spotty coverage
# As can be seen on all, the germ-band does not extend far up
# we expect some inhibiting gene to be doing this IRL
GB[GE.base[:,2] > 50] = 0

# remove in the head domain
GB = GE.not_gene(GB, GE.gene("fkh"))

# Add to embryo
GE.add_expression(GB, 0.2, True, 1) # Germ Band

# Dorsal fold 1
GE.add_expression(GE.get_second_run_stripe(), 0.4, True, 5)
# Second Run Stripe
```

```
# Dorsal fold 2
GE.add_expression(GE.get_fifth_run_stripe(), 0.4, True, 5) # Second Run Stripe

# GE.add_expression(GE.not_gene(GE.or_gene(GE.gene("eve"), GE.gene("run")), GE.gene("Doc2")), 0.2, True, 1) # Germ Band

# add cephalic furrow
GE.add_expression(GE.gene("Dfd"), 0.6, True, 5) # Cephalic Furrow

# combine twist and snail (twist overlaps snail completely)
twist_and_snail = GE.and_gene(GE.gene("twi"), GE.gene("sna"))

GE.add_expression(twist_and_snail, 0.2, True, 2) # Ventral Furrow

# add posterior midgut
GE.add_expression(GE.gene("hkb"), 0.25, True, 4) # PMG

# hkb is expressed both for the Anterior and Posterior invagination
# croc and oc are in the cephalic domain, so I use these to set
# everything in head region back to cell type 0
GE.add_expression(GE.or_gene(GE.gene("croc"), GE.gene("oc")), 0.4, True, 0) # Invert

# Define the PCP from the gradient of the runt gene and save
GE.save("no_q_from_runt", q_from_runt=True)
```

### A8.0.1 Cell types extracted from data

When we say that the cell types were extracted from data, this comes with a couple asterisks:

Any expression in the cephalic region was removed by hand.

**Cephalic furrow** In the data-set there the gene for the Cephalic furrow where not present, but using the website <https://shiny.mdc-berlin.de/DVEX/> we could see that it spatially coincided with *Bfd* which was therefore used as a proxy. **Germ-band** The germ-band was cut off by hand as the *Eve* and

*Run* expressions were very spotty at the top and the germ-band would not extend correctly. We expect there to be a suppressing gene that we did not take into account.

**Ventral furrow** Even though all the cells expressing *twist* & *snail* on the belly lower their apical surface area, they do not constrict indiscriminately. Instead they start out by constricting in the *inner* 8x60 cells. It is believed to be a more stable way of wedging, but is still strange and not fully understood! This meant that a specific rule for the wedging in the ventral region was needed. The inner 8 cells has a wedging constant  $\alpha = 0.5$  while the rest has  $\alpha = 0.2$ .

## A9 Rosette analysis

Convergent Extension is seen as a vital part of the development of many multicellular animals. Therefore multiple different methods of analysis and YYY have been developed. One of the main quantifiers consist of looking at a cluster of neighboring cells that undergo convergent extension. These clusters are called Rosettes. Through laser-ablation it has been shown that the Rosettes (as shown in the diagram on Figure 2.3) can consist of up to twelve internally connected cells [citation needed].

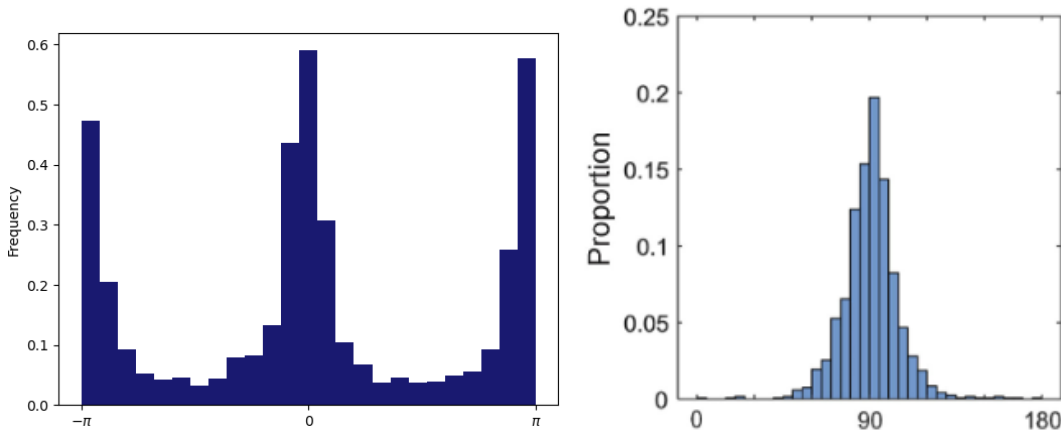


**Figure A.6:** The angular distribution of the newly acquired neighbors in rosettes as found in (left) simulation (in radians) and (right) data (in degrees).

In Figure A.6, the distribution of angles of all found rosette-events can be

seen. Strangely, the distribution is clearly bimodal in horizontal and vertical, where the ground truth has a single peak at the vertical axis.

We believe the lack of malleability in the contours of the cells might be to blame.

In our model, where the equilibrium distance is the same for every direction no matter the pressure exerted, getting a bimodality is predictable. Every time a new pair 'touch' on the up-down axis, they release space for a pair above or below on the perpendicular axis. The lack of anisotropic cell shapes almost forces this discrepancy into being.

## A10 Elements cut for lack of time

### A10.1 Ventral Furrow

We would have loved to quantify the accuracy of our simulated ventral furrow. Doing computer vision cell center fit on 3.2, for example.

### A10.2 Cell surface area

As the changes in cell surface area and percentage of invaginated tissue are known, quantifying the agreement could have helped understand the model better.

### A10.3 Interaction matrix

We have done a bunch of examinations into the mutants. combining different mutations, seeing the second-order interactions, would be an obvious and interesting next step.

### A10.4 Without gene-defined PCP

The Planar Cell Polarity was defined through the *Even skipped* and *Runt* stripes. Seeing the effects this had (compared to simply breaking the in-plane symmetry along the anterior-posterior axis) would have been super interesting.